Collisions and circular motion of spinning magnetized particles orbiting magnetized Kerr black holes

Shokhzod Jumaniyozov,[1,2,*] Saeed Ullah Khan,[3,†] Javlon Rayimbaev,[4,5,6,‡] Inomjon Ibragimov,[7,§] Ahmadjon Abdujabbarov,[8,9,‖] and Zdeněk Stuchlík[10,¶]

[1]*New Uzbekistan University, Movarounnahr Street 1, Tashkent 100000, Uzbekistan*
[2]*Tashkent International University of Education, Imom Bukhoriy 6, Tashkent 100207, Uzbekistan*
[3]*School of Mathematics and Statistics, Fuzhou University, Fuzhou 350108, Fujian, China*
[4]*National University of Uzbekistan, Tashkent 100174, Uzbekistan*
[5]*Urgench State University, Kh. Alimdjan str. 14, Urgench 220100, Uzbekistan*
[6]*Tashkent State Technical University, Tashkent 100095, Uzbekistan*
[7]*Kimyo International University in Tashkent, Shota Rustaveli street 156, Tashkent 100121, Uzbekistan*
[8]*School of Physics, Harbin Institute of Technology, Harbin 150001, People's Republic of China*
[9]*University of Tashkent for Applied Sciences, Str. Gavhar 1, Tashkent 100149, Uzbekistan*
[10]*Research Centre for Theoretical Physics and Astrophysics, Institute of Physics, Silesian University in Opava, Bezručovo nám. 13, CZ-74601 Opava, Czech Republic*

(Received 13 February 2025; accepted 7 August 2025; published 29 August 2025)

Studying spinning magnetized particles in strong gravitational and electromagnetic fields is crucial for understanding astrophysical processes near black holes, particularly in the scenarios of millisecond pulsars orbiting supermassive or intermediate-mass black holes. In this work, we analyze the circular motion and collisions of such particles in the close environment of a magnetized Kerr black hole, considering both spin-curvature and magnetic dipole interactions. Using the Mathisson-Papapetrou-Dixon (MPD) equations, we derive the effective potential governing the circular motion of spinning magnetized particles and investigate the innermost stable circular orbit (ISCO) under the influence of black hole spin, external magnetic fields, and intrinsic particle spin and magnetic dipole moment. The results reveal how the interaction of the magnetic dipole moment with the external field and spin-curvature interactions significantly alter stable orbits, leading to modifications in accretion dynamics. Furthermore, we explore the center-of-mass energy of such high-energy particle collisions, demonstrating that spin and magnetic interactions can amplify collision energies beyond the standard Bañados-Silk-West (BSW) process, with implications for the production of ultrahigh-energy cosmic rays and the formation of jets in active galactic nuclei and low-luminosity galaxies. Our findings may provide theoretical predictions that can be tested using observations of compact objects in strong magnetic fields, such as pulsars near supermassive black holes.

DOI: 10.1103/bl45-hbjm

I. INTRODUCTION

Understanding the motion of spinning particles near black holes (BHs) might provide information on rotating neutron stars, including millisecond pulsars around the supermassive BH Sagittarius A* (Sgr A*). Unfortunately, the GRAVITY Collaboration's recent observations to hunt for pulsars surrounding Sgr A* have revealed no nearby pulsars. The scattered nature of radio waves within the thick plasma region near Sgr A* and the interaction of magnetism caused by the dipole moment of neutron stars and the external magnetic field are possible explanations. Magnetic fields play an essential role in astrophysics. They can be observed and tested for almost every celestial entity and have a major impact on charged particles. Therefore, when studying the motion of test particles, we need to understand how the BH's surroundings' magnetic field interacts with the magnetized items' dipole moment. The existence of magnetic fields around BHs is useful for testing theories of gravity. Wald [1] revolutionized the study of such fields outside Kerr BHs in an asymptotically uniform external magnetic field. Subsequently, several researchers have explored the electromagnetic fields surrounding various BH models in external magnetic fields, including uniform, dipolar, and split monopole magnetic fields [2–12] and neutron stars [13]. External magnetic fields significantly influence the dynamics of test-charged particles, a phenomenon that has been extensively explored in Refs. [14–16]. Furthermore, investigations have been conducted into the

*Contact author: sh.jumaniyozov@newuu.uz
†Contact author: saeedkhan.u@gmail.com
‡Contact author: javlon@astrin.uz
§Contact author: i.ibragimov@kiut.uz
‖Contact author: ahmadjon@astrin.uz
¶Contact author: zdenek.stuchlik@fpf.slu.cz

motion and radiation of charged particles around magnetized BHs, incorporating radiation reaction forces.

Electromagnetic fields near BHs facilitate examining particle dynamics with magnetic dipole momentum and nonzero rotation. Felice and Sorge [17] studied the Schwarzschild BH submerged in an external uniform magnetic field and observed that magnetized particles might travel in stable, nongeodesic, axially circular equatorial orbits with a radius less than the innermost stable circular orbits (ISCO). Later, the research was expanded to incorporate the Kerr BH scenario [18].

The motion of neutral and electrically charged test particles around BHs is a key component in astrophysics. The dynamics of charged particles are exciting because they are crucial to understanding how magnetic fields affect the accretion process. A detailed examination of particle dynamics around BHs and spacetime structure may be found in [19–23]. Investigations into the dynamics of magnetized particles as a test of gravity theories and the structure of spacetime have been carried out in [24–30].

Capture of massless and massive particles by parametrized BHs [31–33]. The orbital and epicyclic frequencies in axially symmetric and stationary spacetime [34–36].

In relativistic astrophysics, particle behavior near BHs reveals a variety of fascinating phenomena. One of the relativistic consequences is the presence of an ISCO, which has been numerically studied for revolving test particles in Schwarzschild and Kerr BHs [37]. The ISCO is the barrier between test particles rotating around the BH and those plunging into it. As a result, it is a crucial characteristic in the study of the accretion disc, as it signifies the inner boundary of the accretion disk in the thin disc model proposed by Shakura and Sunyaev [38,39]. Additionally, it serves as a boundary over the parametrized space, which leads to confined solutions in the thick disc model [40]. Such models have been used extensively as a basis for accretion disc simulations and may be compared with EHT data [41].

The standard Penrose process, proposed for the first time by R. Penrose in 1969 [42] and then by Penrose and Floyd [43], is considered among the most reliable mechanisms for the release of energy from revolving BHs. The central concept of the technique is that a neutral particle undergoes decomposition into two subcomponents inside the ergoregion of spinning BHs. One of these components descends into the center of the BH with negative energy. In contrast, the other component exits the region with positive energy, surpassing the original energy of the parent particle. Theories of gravity have led to the development of several techniques and variations in energy extraction processes over the past few decades. For instance, the Blandford-Znajeck mechanism [44], the Penrose processes involving magnetic and electric fields have been proposed by considering the rotating and charged decayed particles [45–52], and particle acceleration mechanism (BSW) [53] are assumed to be a miniature representation of several energy mechanisms near compact objects in relativistic astrophysics. Zahid *et al.* [54,55] hypothesized that the charged Gauss-Bonnet-AdS BHs might serve as particle accelerators, having potentially significant center-of-mass energy provided the two neutral electrical test particles collide near the horizon.

In our previous paper [56], we first investigated the spinning magnetized particles' motion around Schwarzschild BHs immersed in an externally uniform magnetic field. In this work, as an extension of the previous work, we plan to study the circular motion of spinning magnetized particles around magnetized rotating Kerr BHs. The article is organized as follows: We begin our study by exploring the rotating magnetized particle dynamics near rotating Kerr BHs in Sec. II. Section IV studies the collisions of spinning magnetized particles in the spacetime of magnetized Kerr BHs. Finally, in Sec. V, we summarize our results with concluding remarks. We use the signature $(-,+,+,+)$ for the spacetime metric and geometrized unit system $G = c = 1$. The Latin indices run from 1 to 3, while the Greek indices take values from 0 to 3.

II. MPD EQUATIONS FOR TEST SPINNING MAGNETIZED PARTICLE MOTION

Equations governing the motion of particles possessing both spin and mass, known as the MPD equations, are fundamental in this context. Recent modifications to these equations have been proposed in Refs. [57,58].

For a magnetized Kerr BH, the Mathisson-Papapetrou-Dixon (MPD) equations describe the motion of a spinning test particle with mass m, spin and magnetic dipole moment μ, including spin-curvature coupling and magnetic dipole interactions [59]

$$\frac{Dp^\sigma}{d\tau} = \frac{1}{2}(F^{\alpha\beta;\sigma}\mu_{\alpha\beta} - R^\sigma_{\nu\alpha\beta}S^{\alpha\beta}u^\nu), \tag{1}$$

$$\frac{DS^{\mu\nu}}{d\tau} = p^\mu u^\nu - p^\nu u^\mu, \tag{2}$$

where p^σ is the four-momentum, u^ν is the four-velocity, $F^{\alpha\beta}$ is the electromagnetic field tensor, and $\mu_{\alpha\beta}$ is the magnetic dipole tensor. The first term accounts for the magnetic dipole interaction, while the second term represents spin-curvature coupling. The covariant derivative reads as $D/d\tau \equiv u^\alpha\nabla_\alpha$ and $S^{\alpha\beta}$ is the spin tensor, which is the second rank antisymmetric tensor: $S^{\alpha\beta} = -S^{\beta\alpha}$, describing the spin of particles as follows:

$$S^{\alpha\beta}S_{\alpha\beta} = 2S^2 = 2m^2s^2. \tag{3}$$

This modified MPD equation describes the motion of magnetized particles near a rotating BH, considering both the particle's spin and its interaction with the BH's electromagnetic field. It allows for the study of complex

phenomena, such as spin-orbit coupling and the influence of the BH's magnetic field on the particle's trajectory. The magnetic dipole tensor takes into account the interaction with the magnetic field of the BH

$$\mu_{\alpha\beta} \equiv \epsilon_{\alpha\beta\gamma\delta}\mu^{\gamma}u^{\delta}, \qquad \mu^{\alpha} = \frac{1}{2}\epsilon^{\alpha\beta\gamma\delta}u_{\beta}\mu_{\gamma\delta}. \tag{4}$$

On the other hand, the magnetic dipole moment interacts with the external magnetic field. The four-momentum, accounting for this magnetic interaction, is expressed as [60]

$$p^{\alpha}p_{\alpha} = -m^2\left(1 - \frac{\mathcal{U}}{2m}\right)^2, \tag{5}$$

where, $\mathcal{U} = D^{\alpha\beta}F_{\alpha\beta}$ characterizes the magnetic interaction, appearing as a scalar and $D^{\alpha\beta}$ represents the polarization tensor. Notably, the effective mass of the test particles in the presence of the electromagnetic field becomes $m_{\text{eff}} = m - (1/2)D^{\alpha\beta}F_{\alpha\beta}$, evident from the right-hand side of Eq. (5).

The right-hand side of Eq. (5) is not constant in general due to magnetic interactions. However, for circular orbits, the effective potential ensures stationarity.

The tensors $D^{\alpha\beta}$ and $S^{\alpha\beta}$ for particles possessing both the magnetic dipole moment and spin can be expressed as follows:

$$D^{\alpha\beta} = \eta^{\alpha\beta\sigma\nu}u_{\sigma}\mu_{\nu}, \qquad S^{\alpha\beta} = \eta^{\alpha\beta\sigma\nu}u_{\sigma}s_{\nu}. \tag{6}$$

The rank-4 tensor $\eta^{\alpha\beta\sigma\nu}$ is the Levi-Civita tensor, defined as $\eta^{\alpha\beta\sigma\nu} = \sqrt{-g}\epsilon^{\alpha\beta\sigma\nu}$, where $\epsilon^{\alpha\beta\sigma\nu}$ is the totally antisymmetric symbol and g is the metric determinant.

It is evident from Eq. (6) that when the magnetic moment and spin axes of the particles are orthogonal to the four-velocity (implying that the magnetic dipole moment and spin possess only the vertical θ-component: $\mu^i = (0, \mu^{\theta}, 0)$ and $s^i = (0, s^{\theta}, 0)$), a certain condition must be met for both the spin and polarization tensors

$$S^{\alpha\beta}p_{\beta} = 0, \qquad D^{\alpha\beta}p_{\beta} = 0. \tag{7}$$

A. Spin supplementary conditions and Mathisson-Papapetrou-Dixon equations

When studying the dynamics of spinning particles in curved spacetime, particularly around BHs, spin supplementary conditions (SSCs) play an essential role. These conditions are necessary to close the system of equations arising from the MPD equations and to consistently define the center-of-mass and spin dynamics of the particle. Below, we discuss the most widely used SSCs, including their assumptions, implications, and areas of application [61–63].

1. Tulczyjew-Dixon condition

The Tulczyjew-Dixon SSC is given by

$$S^{\alpha\beta}p_{\alpha} = 0, \tag{8}$$

where $S^{\alpha\beta}$ is the spin tensor and p_{α} is the four-momentum of the particle [64]. This condition ensures that the spin tensor is orthogonal to the four-momentum. Key features of the Tulczyjew-Dixon condition include its suitability for high-energy particles and its ability to define a unique center-of-mass for the particle. This makes it particularly advantageous in relativistic systems, such as the motion of particles in Kerr spacetime, where its consistency with the MPD formalism ensures accurate and reliable results.

2. Mathisson-Pirani condition

The Mathisson-Pirani SSC is expressed as

$$S^{\alpha\beta}u_{\alpha} = 0, \tag{9}$$

where u_{α} is the four-velocity of the particle [65,66]. This condition implies that the spin tensor is orthogonal to the particle's four-velocity. The Mathisson-Pirani condition offers a more flexible description of a particle's dynamics, making it particularly useful for analyzing the helical motion of particles. However, it comes with a notable challenge: it can introduce ambiguities in defining the center-of-mass trajectory, a phenomenon often referred to as the "helical ambiguity."

3. Corinaldesi-Papapetrou condition

The Corinaldesi-Papapetrou SSC is formulated as

$$S^{0i} = 0 \qquad \text{(in the rest frame of the particle)}, \tag{10}$$

where i denotes spatial indices [67,68], this condition assumes that the spin vector is purely spatial in the rest frame of the particle. The characteristics of this approach include several advantages and limitations. It simplifies calculations in static or quasistatic spacetimes, making it particularly effective for slow-moving particles. However, it has limitations as it is not suitable for highly relativistic systems, where more advanced methods are required.

4. Poitou-Dixon condition

This condition modifies the Tulczyjew-Dixon SSC by introducing an arbitrary vector z^{α}

$$S^{\alpha\beta}z_{\alpha} = 0. \tag{11}$$

The vector z^{α} can be chosen to align with specific physical properties of the system [69]. The characteristics of this approach include several advantages and applications. It offers flexibility in choosing the reference frame

and can be adapted to specific scenarios, such as magnetized Kerr BHs. While rarely used in practice, it is valuable in tailored analyses where specific conditions must be taken into account.

5. Ohashi-Kyrian condition

The mathematical formulation of the Ohashi-Kyrian condition is as follows:

$$S^{\alpha\beta}u_\alpha = \lambda u^\beta. \tag{12}$$

Here, λ is a scalar parameter (a specific constant for the spinning particle). The Ohashi-Kyrian condition describes how the spin tensor changes about the particle's motion, enabling flexible solutions in specific systems and scenarios. This SSC introduces a hybrid approach, combining elements of the Tulczyjew-Dixon and Mathisson-Pirani conditions. It ensures that the spin is orthogonal to a dynamically evolving four-vector. The features of this approach include several advantages and challenges. It successfully balances the benefits of the two foundational SSCs, avoiding helical ambiguities while maintaining consistency with relativistic dynamics. However, it comes with the challenge of a more complex mathematical formalism, which can make implementation more difficult.

The appropriate SSC depends on the physical context and the specific characteristics of the studied system. The Tulczyjew-Dixon SSC is preferred for high-energy systems due to its robustness in relativistic regimes. In contrast, the Corinaldesi-Papapetrou SSC may simplify the analysis for low-energy or slow-moving systems. When dealing with helical motion systems, the Mathisson-Pirani SSC is useful for understanding nonlinear trajectories. For more tailored studies, the Poitou-Dixon or Ohashi-Kyrian SSCs can be adjusted to suit specific scenarios.

In conclusion, each SSC offers a distinct perspective on the dynamics of spinning particles, shaping how spin-curvature and spin-magnetic interactions are interpreted. The Tulczyjew-Dixon condition stands out in magnetized Kerr BHs, as it aligns well with relativistic dynamics and uniquely defines the center-of-mass. However, exploring alternative SSCs provides valuable flexibility, enriching the depth of analyses and ensuring a more comprehensive understanding of these complex systems.

Similar to Mathisson's approach, Tulczyjew's method [70,71] provides a framework for handling such scenarios. Additionally, scholars like Moller and others have refined studies concerning the definition of the center-of-mass [72–75].

6. Restricting magnetic dipole moment direction

To simplify the analysis, we assume that the magnetic dipole moment $\mu_{\alpha\beta}$ is aligned along the $\hat{\theta}$ direction and remains static in the equatorial plane ($\theta = \pi/2$). The evolution equation for the dipole moment is,

$$\frac{D\mu_{\alpha\beta}}{d\tau} = \epsilon_{\alpha\beta\gamma\delta}\omega^\gamma \mu^\delta, \tag{13}$$

where ω_γ is the four angular acceleration. In the equatorial plane, the magnetic field is approximately aligned with the $\hat{\theta}$-direction, and the torque term $\mu_{\alpha\beta}F^{\alpha\beta}$ vanishes due to symmetry, ensuring that $\mu_{\alpha\beta}$ remains constant. This assumption is consistent with the setup in [59].

The spatial spin vector s^i is assumed to have only a θ-component, i.e., $s^i = (0, s^\theta, 0)$, implying that the spin is orthogonal to the equatorial plane. This condition is enforced by the Tulczyjew-Dixon SSC, which ensures that the spin tensor $S^{\alpha\beta}$ is orthogonal to the four-momentum p_β. In the equatorial plane ($\theta = \pi/2$), the symmetry of the Kerr spacetime and the alignment of the external magnetic field along the $\hat{\theta}$-direction restrict the spin to the θ-component, as verified in Ref. [18]. On the other hand, when the direction of the magnetic dipole moment of the particle is misaligned with the magnetic field and spin vectors, the particle radiates dipole radiation, loses its kinetic energy, and its orbit is no longer circular. Therefore, in this study, we consider noninclined magnetic dipole moment and spin cases to investigate the circular motion of spinning and magnetized particles.

B. Conserved quantities

Additionally, incorporating the Tulczyjew SSC given by Eq. (7), we obtain conserved quantities associated with the spacetime symmetries. The spacetime metric possesses two Killing vector fields. One generates invariant time translation denoted by ξ^α, while the other produces invariant rotation denoted by ψ^α. Consequently, we derive two conserved quantities, as depicted in the equation below

$$p^\alpha\kappa_\alpha - \frac{1}{2}S^{\alpha\beta}\nabla_\beta\kappa_\alpha = p^\alpha\kappa_\alpha - \frac{1}{2}S^{\alpha\beta}\partial_\beta\kappa_\alpha = \text{const}, \tag{14}$$

where κ^α is a vector related to the two Killing vector fields; i.e., ξ^α or ψ^α.

The conservation of the spin magnitude S and orbital angular momentum L is verified using the Tulczyjew-Dixon SSC ($S^{\alpha\beta}p_\beta = 0$). The spin magnitude is defined as $S^2 = \frac{1}{2}S^{\alpha\beta}S_{\alpha\beta}$. Taking the covariant derivative, we find

$$\begin{aligned}\frac{DS^2}{d\tau} &= S^{\alpha\beta}\frac{DS_{\alpha\beta}}{d\tau} \\ &= S^{\alpha\beta}(p_\alpha u_\beta - p_\beta u_\alpha) = 0,\end{aligned} \tag{15}$$

since $S^{\alpha\beta}p_\alpha = 0$. Thus, S is conserved. For the orbital angular momentum $L = p_\phi - S$, conservation follows

from the conserved total angular momentum $J = p_\phi$, as the spin contribution S is constant under the SSC [73].

III. CIRCULAR MOTION OF SPINNING MAGNETIZED PARTICLES AROUND MAGNETIZED KERR BHS

The spacetime geometry around the Kerr BH can be described using the standard Boyer–Lindquist coordinates with the help of the line element as

$$ds^2 = g_{tt}dt^2 + g_{rr}dr^2 + g_{\theta\theta}d\theta^2 + g_{\phi\phi}d\phi^2 + 2g_{t\phi}dtd\phi,$$

where

$$\begin{aligned} g_{tt} &= -\left(1 - \frac{2Mr}{\Sigma}\right), \\ g_{t\phi} &= -\frac{4Mra\sin^2\theta}{\Sigma}, \\ g_{rr} &= \frac{\Sigma}{\Delta}, \\ g_{\theta\theta} &= \Sigma, \\ g_{\phi\phi} &= \left(\rho^2 + \frac{2Mr}{\Sigma}a^2\sin^2\theta\right)\sin^2\theta, \end{aligned}$$

and

$$\begin{aligned} \Sigma &= r^2 + a^2\cos^2\theta, \\ \Delta &= \rho^2 - 2Mr, \\ \rho^2 &= r^2 + a^2, \end{aligned}$$

where, M is the mass of the rotating BH, and a is the spin parameter, defined as $a = J/M$, where J is the angular momentum.

A. Magnetization of Kerr BH

Here, we consider the external magnetic field as a weak test magnetic field around the rotating BH, which can satisfy the condition $B \ll 10^{19}(M_\odot/M)$ G that cannot contribute to the spacetime curvature of the BH [76].

The magnetic field structure surrounding a BH's horizon can be incredibly complex, particularly near the axis of rotation, where jets may form. Despite the original layout of the magnetic field, a parabolic magnetic field pattern is observed in this region. However, for fundamental estimations, it is often useful to begin with an assumption of an asymptotically uniform magnetic field, as proposed by Wald and widely utilized in significant cosmic investigations.

This work assumes a uniform magnetic field with intensity B, and the field lines aligned along the z-axis to maintain symmetry in the spacetime configuration. This assumption allows us to express the nonzero elements of the electromagnetic potential four-vector A_α, as

$$A^\alpha = \frac{B}{2}(\xi^\alpha_{(\phi)} + 2a\xi^\alpha_{(t)}) - \frac{Q}{2M}\xi^\alpha_{(t)}, \tag{16}$$

where Q represents the induced electric charge within the spacetime of the BH. For BHs lacking any charge, the induced electric charge is absent unless influenced by the spin of the BH and the surrounding magnetic field. This influence generates a maximum electric charge known as the "Wald charge," denoted as $Q_W = 2aB$. This charge creates a potential drop between the central region of the BH and extends to infinity.

The authors of Ref. [18] have estimated that the Wald charge typically remains significantly lower than the critical charge, potentially contributing to the spacetime structure. Hence, in our further analyses, we focus only on chargeless rotating BHs by setting $Q = 0$. Thus, we have the following nonzero electromagnetic field four-potentials:

$$\begin{aligned} A_t &= \frac{B}{2}(g_{t\phi} + 2ag_{tt}), \\ A_\phi &= \frac{B}{2}(g_{\phi\phi} + 2ag_{t\phi}). \end{aligned} \tag{17}$$

The orthonormal components of the magnetic fields can be expressed using the electromagnetic field tensor in the following form:

$$\begin{aligned} B^{\hat{i}} &= \frac{1}{2}\epsilon_{ijk}\sqrt{g_{jj}g_{kk}}F^{jk} \\ &= \frac{1}{2}\epsilon_{ijk}\sqrt{g^{jj}g^{kk}}F_{jk}. \end{aligned} \tag{18}$$

where the symbol ϵ_{ijk} is the three-dimensional Levi-Civita symbol, with $\epsilon_{123} = 1$ and antisymmetric under index permutation. The hatted indices (e.g., $\hat{i}$) denote components in the orthonormal tetrad frame, which is measured by a zero angular momentum observer (ZAMO).

Consequently, we have the vertical components of the magnetic field measured by ZAMO with the velocities $u^\mu_{\rm ZAMO} = \{u^t, 0, 0, u^\varphi\}$, (where $(u^t)^2 = g_{\phi\phi}/(g^2_{t\phi} - g_{tt}g_{\phi\phi})$, $u^\phi = -g_{t\phi}u^t/g_{\phi\phi}$) take the form [77]

$$\begin{aligned} B^{\hat{\theta}} = -\frac{B_0 r\sin^2\theta\sqrt{\Delta}}{\Sigma^2 A}\Bigg\{&\left[\Delta - \left(1 - \frac{M}{r}\right)\Sigma - a^2\sin^2\theta\right] \\ &\times a^2(1 + \cos^2\theta) - \Sigma^2\Bigg\}. \end{aligned} \tag{19}$$

In this subsection, we aim to derive the effective potential for the circular motion of spinning test particles having magnetic dipole moments orbiting magnetized rotating Kerr BHs. Additionally, we consider a scenario in which a test particle possesses both a proper magnetic dipole moment and a spin parameter, with these vectors assumed to be parallel to each other. Moreover, the dipole moment interacts with the external magnetic field in an extra way.

B. Magnetic interaction term

The product's value $D^{\alpha\beta}F_{\alpha\beta}$ can be determined by considering the conditions specified in Eqs. (6) and (7), yielding

$$D^{\alpha\beta}F_{\alpha\beta} = 2\mu^{\hat{\alpha}}B_{\hat{\alpha}}. \tag{20}$$

In our analysis, we assume that the direction of the magnetic dipole moment is perpendicular to the equatorial plane and is parallel to the external magnetic field. Moreover, we consider the equatorial motion of the test spinning magnetized particles, which simplifies our calculations.

Thus, we can express the components of the magnetic dipole moment as $\mu^{\hat{i}} = (0, \mu^{\hat{\theta}}, 0)$, where $\mu^2 = \mu_\alpha \mu^\alpha$ denotes the norm of the dipole magnetic moment. This configuration ensures that the magnetic dipole moment is always parallel to the magnetic field lines and perpendicular to the equatorial plane. Consequently, the interaction term U for the ZAMO takes the form $\mathcal{U} = 2\mu^{\hat{\theta}}B_{\hat{\theta}}$.

At the equatorial plane, the interaction term simplifies to $\mathcal{U} = 2\mu B_0 F(r)$, where

$$F(r) = \frac{a^2M - r^3}{r(r^2+a^2)}\sqrt{1 - \frac{2M}{r} + \frac{a^2}{r^2}}. \tag{21}$$

C. Total angular momentum and energy of spinning particle

Indeed, the interaction of the magnetized particle's magnetic dipole moment solely with the external magnetic field does not disrupt the conservation of quantities p_t and p_ϕ for spinning particles. These quantities can be derived from Eq. (14) as follows:

$$\begin{aligned} -E &= p_t - \frac{1}{2}g_{t\alpha,\beta}S^{\alpha\beta} \\ &= p_t - \frac{1}{2}(g_{tt,r}S^{tr} + g_{t\varphi,r}S^{\varphi r}), \end{aligned} \tag{22}$$

$$\begin{aligned} J &= p_\varphi - \frac{1}{2}g_{\varphi\alpha,\beta}S^{\alpha\beta} \\ &= p_\varphi - \frac{1}{2}(g_{\varphi t,r}S^{tr} + g_{\varphi\varphi,r}S^{\varphi r}). \end{aligned} \tag{23}$$

Where J is the spinning particle's total angular momentum, which can be described as $J = L + S$ ($S = sm$, $L = \mathcal{L}m$).

In reality, in a plane near the equatorial plane, magnetic field lines do not align perpendicular to that plane. According to our assumption, the magnetic dipole moment of the particle is perpendicular to the plane in which its motion occurs. Consequently, the external magnetic field and the magnetic dipole moment are not parallel to each other. A nonzero angle exists between the particle's magnetic moment and the external magnetic field.

It is well-known that the potential energy of magnetic interaction reaches its minimum when this angle is zero, representing an equilibrium state. Consequently, a "nonlinear" force emerges, restoring the magnetized particle to equilibrium. This force initiates nonlinear oscillations of the magnetic dipole around the vertical axis. Subsequently, the particle emits electromagnetic waves, leading to either its gravitational collapse or its escape from the central object as it loses energy and angular momentum. Hence, the motion of magnetized particles at a nonequatorial plane proves unstable.

Therefore, to simplify our analysis and focus on more stable scenarios, we confine our attention to the equatorial plane, where $\theta = \pi/2$. Using the Eq. (3) and Eq. (7) conditions, one may get the equations below,

$$S^{tr} = -\frac{p_\varphi s}{\sqrt{g_{rr}(g_{t\phi}^2 - g_{tt}g_{\phi\phi})}}, \tag{24}$$

$$S^{\varphi r} = \frac{p_t s}{\sqrt{g_{rr}(g_{t\phi}^2 - g_{tt}g_{\phi\phi})}}. \tag{25}$$

Starting from this point, we adopt a unit convention where radial coordinates and momenta are rescaled by the BH mass M, i.e., $r \to r/M$, $J \to J/(mM)$.

The Eqs. (24) and (25) can be described as

$$-E = p_t - \frac{s}{2r}(p_\varphi g_{tt,r} + p_t g_{t\varphi,r}), \tag{26}$$

$$J = p_\varphi - \frac{s}{2r}(-p_\varphi g_{t\varphi,r} + p_t g_{\varphi\varphi,r}), \tag{27}$$

and by solving Eqs. (26) and (27) we get

$$p_t = \frac{Js - E(as + r^3)}{r^3 - s^2}, \tag{28}$$

$$p_\varphi = \frac{Es(a^2 - r^3) + J(r^3 - as)}{r^3 - s^2}. \tag{29}$$

D. Deriving effective potential for circular motion

Now, we use Eqs. (5) and (20) to get the equation for the effective potential of the spinning magnetized particle,

$$\begin{aligned} (p^r)^2 = -g^{rr}[&g^{tt}p_t^2 + g^{\varphi\varphi}p_\varphi^2 + 2g^{t\varphi}p_t p_\varphi \\ &+ m^2(1 - \beta F(r))^2], \end{aligned} \tag{30}$$

where $\beta = \mu B_0/m$ is the magnetic interaction (coupling) parameter that describes the interaction between the dipole moment and the magnetic field.

$$\rho(u^r)^2 = \alpha\mathcal{E}^2 + \delta\mathcal{E} + \gamma, \tag{31}$$

where $\mathcal{E}$ is the specific angular momentum, and new notations are

$$\begin{aligned}
\rho &= (r^3 - S^2)^2(2rg_{\phi\phi} - \Sigma(g_{t\phi}^2 + g_{\phi\phi})),\\
\alpha &= 2rS^2(a^2 - r^3)^2 + S(a^2 - r^3)(S(r^3 - a^2) + 2g_{t\phi}(aS + r^3)) + g_{\phi\phi}(aS + r^3)^2,\\
\delta &= 2J(g_{t\phi}(S^2(r^3 - 2a^2) + r^6) + S(a^2 - r^3)(aS - r^3) - Sg_{\phi\phi}(aS + r^3)) - 2rS(r^3 - a^2)(r^3 - aS),\\
\gamma &= \{2J^2Sg_{t\phi}(r^3 - aS) + J^2(r^3 - aS)^2 + g_{\phi\phi}(\beta F(r^3 - S^2) - JS - r^3 + S^2)(\beta F(r^3 - S^2) + S(J + S) - r^3)\\
&\quad + (\beta F - 1)^2 g_{t\phi}^2(r^3 - S^2)^2\} + 2J^2r(r^3 - aS)^2 + 2r(\beta F - 1)^2 g_{\phi\phi}(r^3 - S^2)^2. \qquad (32)
\end{aligned}$$

We can rewrite Eq. (31) as,

$$(u^r)^2 = \frac{\alpha}{\rho}(\mathcal{E} - V_+)(\mathcal{E} - V_-). \qquad (33)$$

Hence, it is possible to define the effective potential for the circular motion of the spinning magnetized particles $p^r = 0$ as a solution of Eq. (33) in the following form [78,79]:

$$V_\pm = \frac{-\delta \pm \sqrt{\delta^2 - 4\alpha\gamma}}{2\alpha}. \qquad (34)$$

We can define new variables as $s \to s/M = S/(mM)$.

One can see from Eq. (33) that to have $(u_r)^2 \geq 0$, the specific energy of the test particles must satisfy the conditions: (i) $\mathcal{E} < V_-$ or (ii) $\mathcal{E} > V_+$.

Hereafter, we focus on the case of test particles spinning with positive energy, which coincides with the effective potential $V_{\text{eff}} = V_+$. Here, we redefine the effective potential as,

$$V_{\text{eff}} = \frac{-\delta + \sqrt{\delta^2 - 4\alpha\gamma}}{2\alpha}. \qquad (35)$$

Indeed, due to the complexity of the expression for the potential considering the combined effects of spin and magnetic interactions, graphical analysis proves to be a valuable tool for understanding the behavior of test particles spinning and magnetized in radial motion. By plotting the effective potential as a function of the radial coordinate, we can visualize how the interplay between spin and magnetic interactions, as well as their combined effects, influences the particle's motion. We can explore these plots by exploring different parameter values and scenarios to gain insights into the particles' behavior.

Specifically, we can examine how spin and magnetic interactions alter the shape and depth of potential wells or barriers, indicating regions where particles are attracted toward or repelled from the central object. Additionally, we can investigate how varying the strength of the magnetic field or the particle's spin affects the stability of orbits and the overall dynamics of the system. Graphical analysis allows us to discern intricate patterns and dependencies in the behavior of spinning and magnetized particles, providing valuable insights that may not be immediately apparent from the mathematical expressions alone.

An interesting point is in which values of the spin and magnetic interaction parameters the effective potential (35) takes positive values. Let us make simple analyses: since it depends on the sign of the complicated notations α, δ, and γ. Let us make simple algebraic analyses in which cases V_{eff} is only positive. Here are the combinations of sing of the notations where $V_{\text{eff}} > 0$: at $\delta > 0$ cases: $\alpha > 0$ & $\gamma < 0$ and $\alpha < 0$ & $\gamma < 0$, also at $\delta < 0$ cases: $\alpha > 0$ & $\gamma > 0$ and $\alpha < 0$ & $\gamma < 0$.

Figure 1 illustrates the radial dependence of the effective potential for the radial motion of a magnetic spinning particle, considering various values of the magnetic parameter β and the spin of the particle s. The results are considered for two cases here: (I) the first case is in the upper panel of Fig. 1 for the normal rotation of the BH ($a = 0.3$) around its axis, and (II) the second case is in the lower panel of Fig. 1 for the rapid rotation of the BH ($a = 0.9$). In comparison, the specific angular momentum of the particle is constant, with a value of $\mathcal{L} = 4.3$.

In the upper-left panel of Fig. 1, the effective potential of the neutral spinning particle is shown as a function of radial distance. The plot demonstrates that the maximum effective potential increases as the particle's spin increases. The upper-middle panel of the figure indicates that the magnetic parameter β significantly affects the effective potential; as β increases, the effective potential diminishes, as shown. On the upper right, the radial dependence of the effective potential for a magnetized particle with normal spin is shown. Additionally, the three figures in the lower panel display different values of the magnetic parameter β and the particle's spin s for a rapidly rotating BH.

E. Superluminal bound

In this section, we explore the concept of a superluminal bound. As previously mentioned, the four-velocity u^α and four-momentum p^α of a particle are not aligned with the spin of the particle. For a massive particle, the four-velocity satisfies the condition

$$u^\alpha u_\alpha = -1, \qquad (36)$$

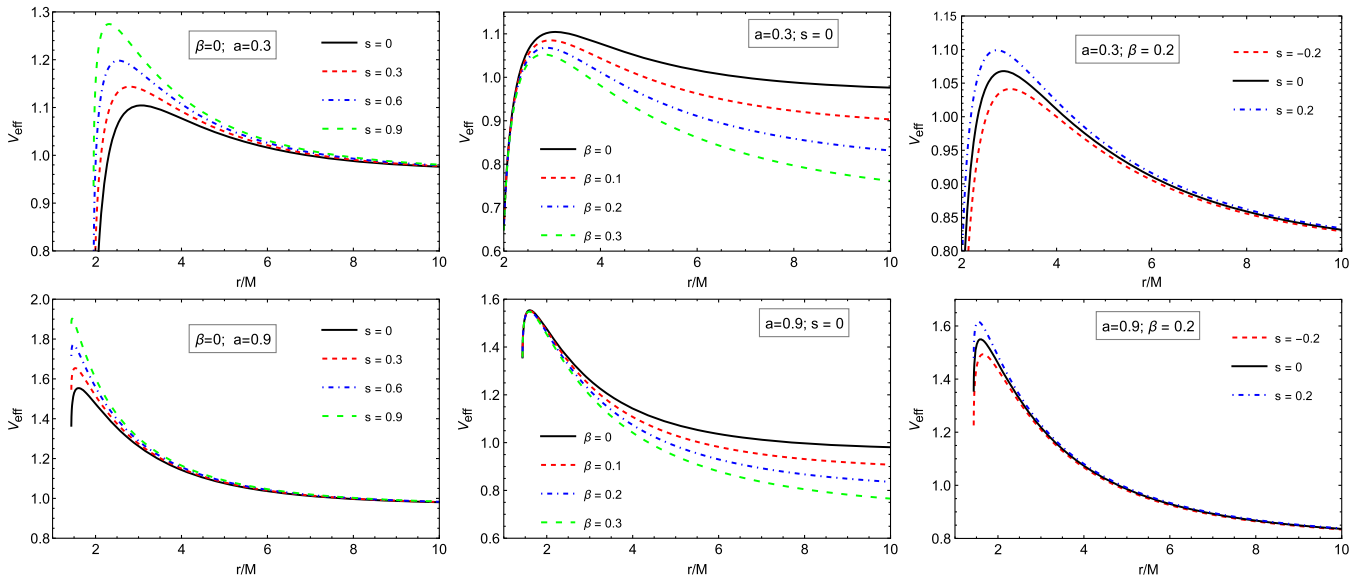

FIG. 1. The radial dependence of the effective potential for various values of the magnetic parameter β and the particle's spin s. We consider $\mathcal{L} = 4.3M$ and two cases on the basis of BH spin, i.e., the normal rotation of the BH ($a = 0.3$) and rapid rotation of the BH ($a = 0.9$).

ensuring that the trajectory of the particle is timelike [73]. This shows that as particles approach a BH, their velocities increase, becoming faster than the speed of light in a vacuum, and as a result they may eventually become spacelike, meaning their motion becomes nonphysical or superluminal. The superluminal condition plays a crucial role in describing the motion of spinning particles, as it allows us to differentiate between timelike and spacelike trajectories. Essentially, this condition imposes a limit on the spin of the particles. Helpful discussions on the superluminal bound can be found in the work of [80,81].

The criterion for a spinning, magnetized particle to follow a timelike trajectory is given by $u^\alpha u_\alpha < 0$. Alternatively, this condition can be expressed as:

$$\frac{u^\alpha u_\alpha}{(u^t)^2} = g_{tt} + 2g_{t\varphi}\frac{d\varphi}{dt} + g_{rr}\left(\frac{dr}{dt}\right)^2 + g_{\varphi\varphi}\left(\frac{d\varphi}{dt}\right)^2 < 0. \quad (37)$$

With the superluminal bound in place, the components of the symmetric spin tensor $S^{\alpha\beta}$ can be determined using the approach outlined in Ref. [82]. This approach involves applying the MPD equations (1) alongside the Tulczyjew-SSC. In particular, the second MPD equation is utilized to compute $DS^{tr}/d\lambda$, $DS^{t\varphi}/d\lambda$, and $DS^{r\varphi}/d\lambda$, which results in a system of equations for the nonzero components of $S^{\alpha\beta}$. This system can then derive the radial and azimuthal components of the four-velocity vector,u^r and u^φ.

$$\frac{DS^{tr}}{d\lambda} = p^t u^r - u^t p^r, \quad (38)$$

$$\frac{DS^{t\varphi}}{d\lambda} = p^t u^\varphi - u^t p^\varphi, \quad (39)$$

$$\frac{DS^{r\varphi}}{d\lambda} = p^r u^\varphi - u^r p^\varphi. \quad (40)$$

By selecting a unique gauge where $\lambda = t$, as described in Ref. [82], the system of equations for the nonzero components of $S^{\alpha\beta}$ can be simplified to a single equation involving only $S^{\varphi r}$. This simplification arises from the MPD equations, which enable the derivation of constraints on the components of $S^{\alpha\beta}$.

$$\frac{dr}{dt} = \frac{u^r}{u^t} = \frac{\mathcal{C}p_r}{\mathcal{B}p_t + \mathcal{D}p_\varphi},$$
$$\frac{d\varphi}{dt} = \frac{u^\varphi}{u^t} = \frac{\mathcal{D}p_t + \mathcal{A}p_\varphi}{\mathcal{B}p_t + \mathcal{D}p_\varphi}, \quad (41)$$

with

$$\mathcal{A} = g^{\varphi\varphi} + R_{trrt}\left(\frac{S^{\varphi r}}{p_t}\right)^2, \quad (42)$$

$$\mathcal{B} = g^{tt} + R_{\varphi rr\varphi}\left(\frac{S^{\varphi r}}{p_t}\right)^2, \quad (43)$$

$$\mathcal{C} = g^{rr} + R_{\varphi tt\varphi}\left(\frac{S^{\varphi r}}{p_t}\right)^2, \quad (44)$$

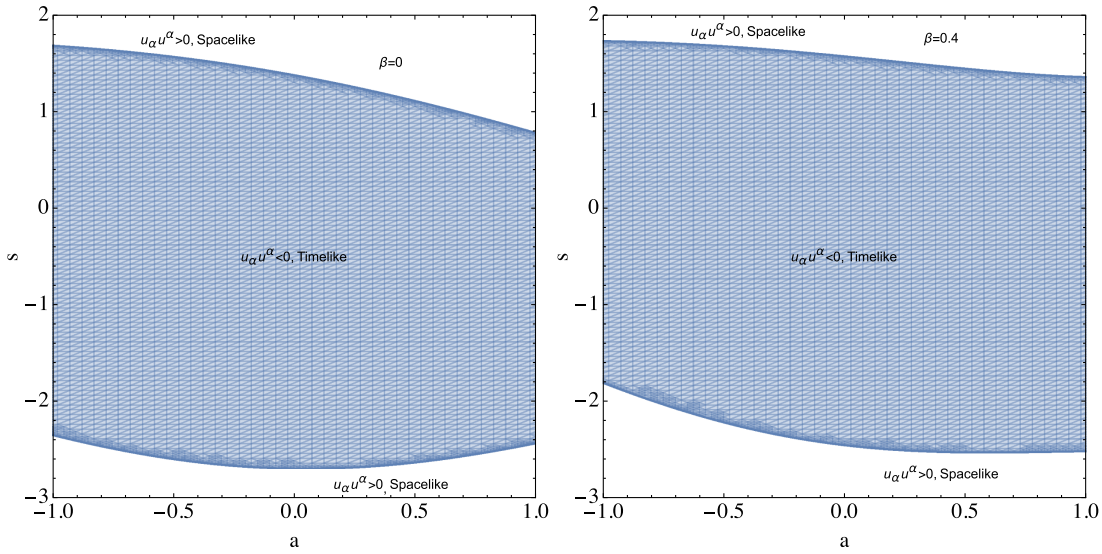

FIG. 2. Region plots of $\mathcal{F}$ given in Eq. (47) for timelike and spacelike spacetimes, with $M = 1$ in the absence (left panel) and presence (right panel) of magnetic dipole interaction.

$$\mathcal{D} = g^{t\varphi} + R_{tr\varphi r}\left(\frac{S^{\varphi r}}{p_t}\right)^2. \tag{45}$$

By substituting Eq. (41) into the superluminal bound condition (37), we can derive a condition that determines when the superluminal bound holds.

$$\mathcal{F} = g_{tt}(\mathcal{B}p_t + \mathcal{D}p_\varphi)^2 + g_{rr}(\mathcal{C}p_r)^2 + 2g_{t\varphi}(\mathcal{D}p_t + \mathcal{A}p_\varphi) \times (\mathcal{B}p_t + \mathcal{D}p_\varphi) + g_{\varphi\varphi}(\mathcal{D}p_t + \mathcal{A}p_\varphi)^2 < 0, \tag{46}$$

By applying the conservation of four-momentum, as shown in Eq. (5), the superluminal bound condition can be simplified.

$$\mathcal{F} = \mathcal{X}\left(\frac{p_t}{m}\right)^2 + 2\mathcal{Y}\left(\frac{p_t}{m}\right)\left(\frac{p_\varphi}{m}\right) + \mathcal{Z}\left(\frac{p_\varphi}{m}\right)^2 - \mathcal{G} < 0, \tag{47}$$

with

$$\begin{aligned}
\mathcal{X} &= g_{tt}\mathcal{B}^2 + 2g_{t\varphi}\mathcal{B}\mathcal{D} + g_{t\varphi}\mathcal{D}^2 - g^{tt}g_{rr}^2\mathcal{C}^2,\\
\mathcal{Y} &= g_{tt}\mathcal{B}\mathcal{D} + g_{t\varphi}(\mathcal{A}\mathcal{B} + \mathcal{D}^2) + g_{\varphi\varphi}\mathcal{A}\mathcal{D} - g^{t\varphi}g_{rr}^2\mathcal{C}^2,\\
\mathcal{Z} &= g_{tt}\mathcal{D}^2 + 2g_{t\varphi}\mathcal{A}\mathcal{D} + g_{\varphi\varphi}\mathcal{A}^2 - g^{\varphi\varphi}g_{rr}^2\mathcal{C}^2,\\
\mathcal{G} &= g_{rr}^2\mathcal{C}^2.
\end{aligned} \tag{48}$$

A more detailed discussion on the superluminal bound and its role can be found in Refs. [81]. According to these references, for timelike particles to move in a circular orbit, the condition $\mathcal{F} < 0$ must be satisfied.

In Fig. 2, we show region plots of particle and BH spins for timelike and spacelike spacetimes in the presence (right panel) and absence (left panel) of magnetic dipole interaction. It is observed that the spin range for timelike spacetime expanded in the extreme rotating Kerr BH case, at $a = 1$; however, when $a = -1$, the negative values of s decrease and become larger than $s > -2$.

F. Stable circular orbits

The circular orbits around rotating Kerr BHs are a fundamental concept in understanding the behavior of test particles in the vicinity of these enigmatic objects. To investigate these orbits, we use a set of conditions that describe the stationary, stable motion of particles in the curved spacetime surrounding a rotating BH. The following equations define these conditions:

$$\dot{r} = 0, \qquad V_{\text{eff}} = \mathcal{E}, \qquad \frac{\partial V_{\text{eff}}}{\partial r} = 0. \tag{49}$$

Here, $\dot{r} = 0$ ensures no radial velocity, the particle is constrained to a circular orbit. The second condition, $V_{\text{eff}} = \mathcal{E}$, equates the effective potential of the particle to its conserved energy $\mathcal{E}$, ensuring that the particle has precisely the right amount of energy to remain in orbit without moving radially inward or outward [83].

The third condition, $\frac{\partial V_{\text{eff}}}{\partial r} = 0$, identifies the critical points in the effective potential, and these points must correspond to minima for the orbit to be stable [84,85]. Together, these conditions describe the stable circular orbits of test particles in Kerr spacetime. The stability of such orbits depends not only on the effective potential but also on the curvature of spacetime and the rotation of the BH itself. The angular momentum and energy of the particle in these orbits can be calculated precisely from the derived expressions, providing essential insights into the particle's motion around the BH [86].

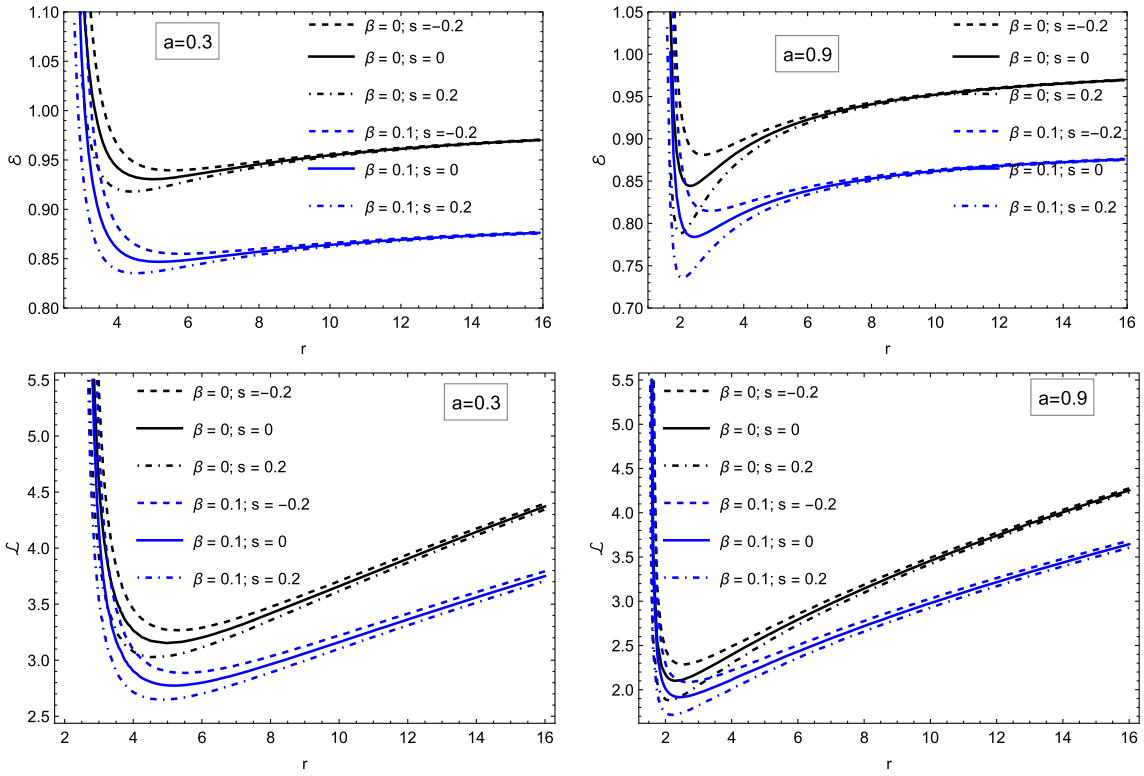

FIG. 3. Radial dependence of energy (left panel) and angular momentum (right panel) at circular orbits of the spinning particle for different values of the spin and magnetic parameter. Here, we assume $M = 1$; the graphs show that the specific energy and specific angular momentum reach their minimum values when the BH rotates rapidly.

The rotation of the BH, characterized by the spin parameter a, plays a crucial role in the behavior of circular orbits. In particular, in prograded orbits (corotating orbits), particles move in the same direction as the BH's spin. Spacetime dragging allows the particle to orbit closer to the event horizon [87]. In retrograde orbits (counterrotating orbits), particles orbit opposite the BH's spin. These orbits are pushed farther out due to the opposing effects of the BH's spin [88].

The ISCO represents the critical boundary beyond which particles can no longer maintain stable circular motion. This boundary is crucial in astrophysical processes, including the structure of accretion disks, the formation of relativistic jets, and the generation of gravitational waves in compact binary systems.

By deriving the expressions for the energy and angular momentum of particles in circular orbits, we gain a deeper understanding of the physical principles governing motion around rotating BHs [89]. These insights are crucial for interpreting observational data from high-energy astrophysical phenomena and advancing our knowledge of the nature of BHs.

Figure 3 presents the radial distributions of energy and angular momentum for circular orbits of test particles with spin and magnetization around magnetized Kerr B Hs, considering various spin and magnetic interaction parameter values. The left panel presents the values of the specific energy and specific angular momentum for a normally ($a = 0.3$) rotating BH. The right panel displays the values of the specific energy and specific angular momentum for a rapidly ($a = 0.9$) rotating BH. It can be concluded from the graphs that the specific energy and specific angular momentum reach their minimum values in the presence of a rapidly rotating BH.

G. Innermost stable circular orbits

The ISCO plays a vital role in understanding the motion of particles around rotating BHs, as described by the Kerr metric. For spinning magnetized particles orbiting a Kerr BH, identifying the ISCO requires analyzing how the magnetic parameter β and the BH's spin influence the particle's motion.

To find the ISCO for spinning magnetized particles, the following three conditions must be satisfied:

(1) The particle must have no radial motion, meaning it follows a perfectly circular orbit:

$$\frac{dr}{d\tau} = 0 \quad \text{or} \quad V_{\text{eff}}(r) = \mathcal{E}. \tag{50}$$

where $V_{\text{eff}}(r)$ is the effective potential, and $\mathcal{E}$ is the conserved energy of the particle [83].

(2) The radial acceleration must vanish to ensure stability

$$\frac{d^2r}{d\tau^2} = 0 \quad \text{or} \quad \frac{dV_{\text{eff}}}{dr} = 0. \tag{51}$$

(3) At the ISCO, the orbit becomes marginally stable, which requires

$$\frac{d^2V_{\text{eff}}}{dr^2} = 0. \tag{52}$$

Together, these three conditions determine the precise location of the ISCO [84].

Spin effects introduce additional terms due to spin-curvature coupling, which is more complex in Kerr spacetime. Due to the complexity introduced by the BH's rotation and the particle's spin, this system cannot be solved analytically. These methods allow precise determination of the ISCO radius for given values of the BH's spin a and the particle's spin s [88].

The ISCO marks the inner edge of the accretion disk around a BH. Material inside this radius spirals inward and falls into the BH [86]. Processes near the ISCO contribute to the generation of relativistic jets. The ISCO influences the gravitational wave signals emitted during the mergers of compact objects.

The ISCO radius decreases with increasing BH spin for prograde orbits and increases for retrograde orbits. For a maximally rotating Kerr BH, the ISCO for prograde orbits shrinks to the event horizon, while it moves farther out for retrograde orbits [89].

Determining the ISCO in Kerr spacetime is essential for understanding the dynamics of spinning particles around rotating BHs. By solving the system of nonlinear equations numerically, one can accurately find the ISCO radius, which has significant implications for accretion disk structure, jet formation, and gravitational wave physics [83].

Figure 4 illustrates the specific angular momentum ($\mathcal{L}_{\text{ISCO}}$) and the specific energy ($\mathcal{E}_{\text{ISCO}}$) of the particles at the ISCO and r_{ISCO} for normally ($a = 0.3$) rotating BH. The top panel of Fig. 4 shows the dependence of r_{ISCO}, $\mathcal{E}_{\text{ISCO}}$, and $\mathcal{L}_{\text{ISCO}}$ on the particle's spin s for different values of the magnetic interaction parameter β. As seen in the figure, as β increases, r_{ISCO} also increases, while $\mathcal{L}_{\text{ISCO}}$ and $\mathcal{E}_{\text{ISCO}}$ decrease. The middle panel of Fig. 4 illustrates the dependence of r_{ISCO}, $\mathcal{E}_{\text{ISCO}}$, and $\mathcal{L}_{\text{ISCO}}$ on the magnetic

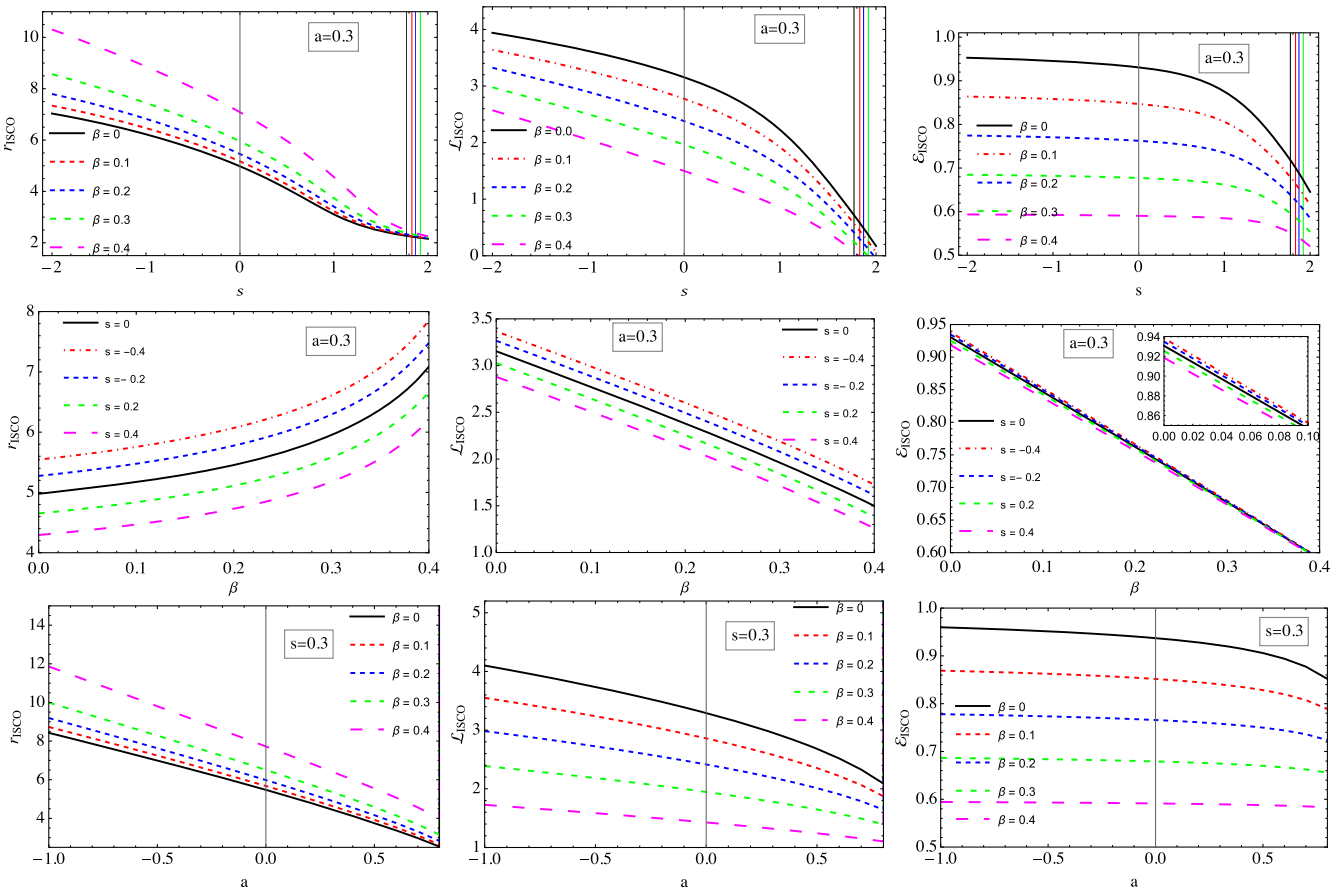

FIG. 4. Dependence of ISCO radius, specific angular momentum, and the specific energy at the ISCO radius on the particle's spin for the different magnetic parameter values β, and $M = 1$. β contributes to r_{ISCO}, whereas it diminishes both of the $\mathcal{L}_{\text{ISCO}}$ and $\mathcal{E}_{\text{ISCO}}$.

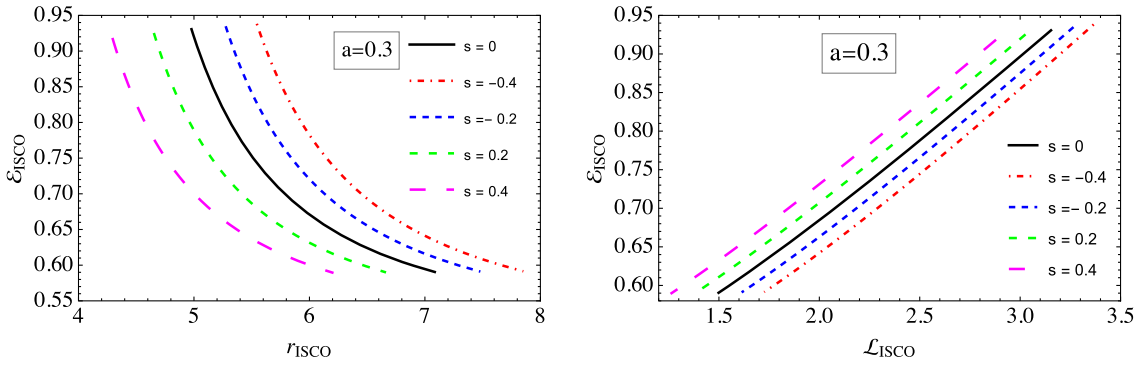

FIG. 5. ISCO radius, the specific energy and specific angular momentum of the particles at ISCO as a function of β for different values of s, and $M = 1$.

interaction parameter β for different values of the particle's spin s. It can be seen that as the particle's spin increases, the values of $r_{\rm ISCO}$, $\mathcal{E}_{\rm ISCO}$, and $\mathcal{L}_{\rm ISCO}$ decrease. In the bottom panel, the graphs of $r_{\rm ISCO}$, $\mathcal{L}_{\rm ISCO}$, and $\mathcal{E}_{\rm ISCO}$ as functions of the BH's spin are shown for different values of β. As depicted in the figure, an increase in β leads to a rise in $r_{\rm ISCO}$, whereas $\mathcal{L}_{\rm ISCO}$ and $\mathcal{E}_{\rm ISCO}$ exhibit a decreasing trend.

The first left panel of Fig. 5 depicts the correlation between the specific energy and the radius at the ISCO, considering various values of the particle's spin s. Larger values of the particle's spin s require the magnetized particle to move in the ISCO with reduced energy. The graph on the right side of Fig. 5 illustrates the dependence of the particle's energy at the ISCO on its angular momentum, presented for various values of the particle's spin.

Figure 6 illustrates the relationship between the ISCO radius, specific energy, and specific angular momentum of spinning magnetized particles orbiting a magnetized Kerr BH, parametrized by the magnetic interaction parameter. The results are obtained for a fixed value of the spin parameter $s = 0.3$, which accounts for the spin-curvature interaction in the particle's motion.

The left panel of Fig. 6 shows the variation of the ISCO radius. The ISCO radius with the magnetic interaction parameter β. It is evident that as β increases, the ISCO radius also increases. This trend indicates that stronger magnetic interactions tend to shift the ISCO outward, suggesting that the combined effects of spin and magnetization introduce repulsive interactions that stabilize circular orbits at larger radii.

The middle panel presents the dependence of the specific energy $E_{\rm ISCO}$ of the particle at the ISCO on β. The results indicate a decreasing trend in the energy required for stable circular motion as β increases. This behavior can be attributed to the energy contributions from the magnetic dipole interaction, which alters the balance of forces governing the stability of circular orbits. The right panel depicts the variation of the specific angular momentum $\mathcal{L}_{\rm ISCO}$ as a function of β. A clear decreasing trend indicates that magnetized particles require lower angular momentum to maintain stable orbits at the ISCO as the magnetic interaction strengthens. This effect is particularly relevant in understanding how magnetized accretion flows behave in the presence of strong magnetic fields around rotating BHs.

Lastly, Fig. 7 illustrates the connection between the magnetic parameter and the spin of the particle for a constant circular orbit ($r_{\rm ISCO} = 6M$). The graph shows that the particle's rotation slows as the BH's spin increases. This figure is also significant as it highlights the combined effects of spin and magnetic interaction on the stability of circular orbits around a magnetized Kerr BH. Additionally, it illustrates how the allowed range of the spin parameter

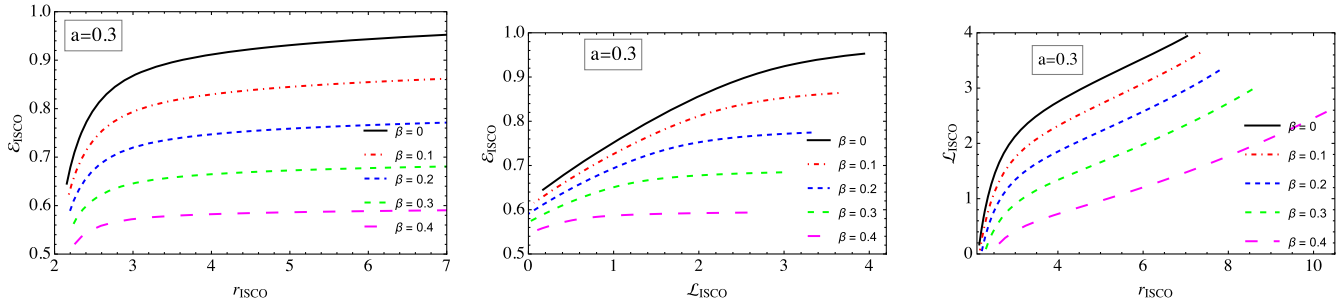

FIG. 6. Dependence between ISCO radius, specific energy, and specific angular momentum of the particles at ISCO for different values of β. Here, we have set $s = 0.3$ and use $M = 1$.

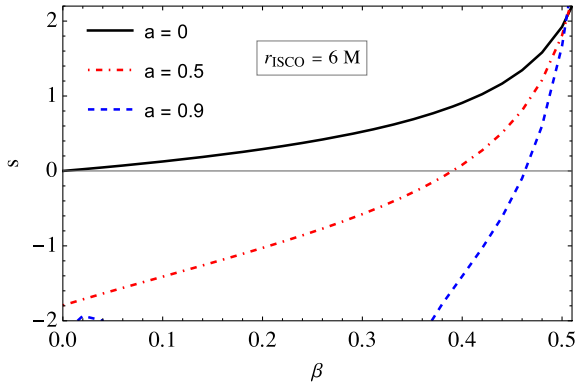

FIG. 7. The relationships between the spin and magnetic parameters providing the ISCO radius as $r = 6M$.

varies with the magnetic interaction parameter to satisfy the ISCO condition.

As Fig. 7 shows, for higher values of the BH spin, the region of parameter space where ISCO is possible shifts significantly. In particular, as the BH's spin increases, the corresponding particle's spin value decreases, which is necessary to maintain a stable orbit. This indicates that strong frame-dragging effects dominate higher spins, resulting in more compact orbits for spinning, magnetized particles. For lower values of the spin parameter, the ISCO remains at larger radii, and the dependence on β and s is less pronounced. When the magnetic interaction parameter increases, the ISCO solutions shift toward higher spin values, indicating that the magnetic force provides an additional stabilizing effect on the orbit. This result has important astrophysical implications. It suggests that the combined influence of magnetic fields and spin-curvature coupling may play a crucial role in the structure of accretion disks, the formation of relativistic jets, and the potential observational signatures in strong gravity regimes. The findings are particularly relevant to neutron stars, magnetized accretion disks, and active galactic nuclei hosting spinning BHs.

IV. COLLISIONS OF SPINNING MAGNETIZED PARTICLES

The study of high-energy particle collisions near BHs has gained significant attention due to its potential to explain some of the most energetic phenomena in the universe. One of the key mechanisms in this field is the Bañados-Silk-West (BSW) process, first proposed by Bañados, Silk, and West in 2009 [90]. This process explores how particles colliding near BH's event horizon can achieve high center-of-mass energies, potentially allowing energy extraction from BH.

The BSW process describes how particles can be accelerated to arbitrarily high energies when they collide near the event horizon of a rotating BH. The process is most effective in extreme Kerr BHs, where the BH spins at its maximum allowed rate. In this scenario, if two particles fall into the BH and collide near the event horizon, the energy in the center-of-mass frame can become extremely large. This offers a theoretical method for extracting energy from a BH.

Further studies have extended the BSW process to nonextremal and more general BH solutions, including the external fields and different types of matter.

Before the BSW process, Roger Penrose introduced the concept of energy extraction from rotating BHs in 1969. The Penrose process involves a particle entering the ergoregion of a rotating BH, where the BH's rotation drags the spacetime. Within the ergoregion, a particle can split into two: one particle falls into the BH with negative energy (relative to an observer at infinity), and the other escapes to infinity with more energy than the original particle.

The efficiency of this process is directly linked to the size of the ergoregion. A larger ergoregion allows for more efficient energy extraction. However, the process stops when the ergoregion vanishes (as in the case of nonrotating BHs).

The magnetic Penrose process (MPP) extends this idea by considering the effects of an external magnetic field around the BH. Introduced by Wagh and Dadhich, the MPP demonstrates that the presence of a magnetic field can significantly enhance energy extraction efficiency. Near magnetized supermassive BHs, charged particles such as protons and ions can be accelerated to ultrahigh energies, reaching up to 10^{22} eV. This mechanism could explain the origin of the highest-energy cosmic rays observed in the Universe.

Studies have shown that head-on collisions near BHs are particularly efficient for energy extraction. In such scenarios, two particles approach each other from opposite directions, maximizing their relative velocity and, consequently, the center-of-mass energy. This configuration enables a more efficient conversion of gravitational energy into kinetic energy, making it a favorable setup for studying high-energy processes.

In the context of spinning magnetized particles, the dynamics become even more complex and interesting. The spin of a particle and its interaction with external magnetic fields introduce additional forces, such as spin-curvature coupling and Lorentz forces, which influence the motion and collision dynamics. These effects can either enhance or suppress the energy of collisions, depending on the alignment of the particle's spin with the BH's spin and the magnetic field configuration [91].

A. Critical angular momentum

Understanding the behavior of particles near a BH is essential for exploring high-energy astrophysical processes, such as particle collisions and accretion dynamics. Before delving into the study of center-of-mass energy in collisions involving spinning and magnetized particles, it is

crucial to determine the conditions under which particles can move from infinity toward the BH and interact near its event horizon. The particle's angular momentum largely influences this motion [83]. For a particle to move closer to the BH, its radial motion must satisfy the condition

$$\dot{r}^2 \geq 0. \tag{53}$$

This condition ensures that the particle's motion is physically allowed and that it can continue moving inward without being halted by an effective potential barrier. From the radial equation of motion, it becomes evident that an increase in the particle's angular momentum leads to a decrease in its radial velocity. The centrifugal force associated with higher angular momentum counteracts the gravitational pull of the BH. As a result, particles with sufficiently large angular momentum cannot move closer to the BH and are instead forced to orbit at a safer distance. We introduce the concept of critical angular momentum to identify the precise threshold at which this transition occurs. This is the maximum angular momentum a particle can have while still being able to approach the BH. It can be determined by solving the following system of equations simultaneously.

The critical angular momentum $\mathcal{L}_{\rm cr}$ is obtained by solving

$$\dot{r}^2 = 0, \qquad \frac{d\dot{r}^2}{dr} = 0, \tag{54}$$

The first condition, $\dot{r}^2 = 0$, signifies that the particle reaches a turning point in its radial motion, meaning it momentarily stops moving inward or outward. The second condition, $\frac{d\dot{r}^2}{dr} = 0$, ensures that this turning point is an inflection point, indicating the transition between possible and forbidden motion.

Solving these equations provides the critical angular momentum value, which separates particles capable of falling into the BH from those that remain in stable orbits farther away.

One can immediately have the following form of radial velocity with respect to the angular momentum ($\mathcal{L}$)

$$h(\dot{r}^2) = a\mathcal{L}^2 + b\mathcal{L} + c, \tag{55}$$

or equivalently, we have

$$\dot{r}^2 = \frac{a}{h}(\mathcal{L} - \mathcal{L}_+)(\mathcal{L} - \mathcal{L}_-). \tag{56}$$

with the solutions

$$\mathcal{L}_{\rm cr} = \mathcal{L}_\pm = \frac{-b \pm \sqrt{b^2 - 4ac}}{2a}, \tag{57}$$

where $\pm$ corresponds to clockwise and anticlockwise orbits and

$$\begin{aligned}
h &= -\frac{g^{rr}}{(r^3 - S^2)^2} \\
a &= (g^{\phi\phi} r^6 + 2g^{t\phi} r^3 S - 2a g^{\phi\phi} r^3 S + g^{tt} S^2 - 2a g^{t\phi} S^2 + a^2 g^{\phi\phi} S^2) \\
b &= (-2g^{t\phi} r^6 - 2g^{tt} r^3 S + 2a^2 g^{\phi\phi} r^3 S - 2g^{\phi\phi} r^6 S - 2a g^{tt} S^2 + 4a^2 g^{t\phi} S^2 - 2a^3 g^{\phi\phi} S^2 - 2g^{t\phi} r^3 S^2 + 2a g^{\phi\phi} r^3 S^2) \\
c &= (r^6 + g^{tt} r^6 + 2a g^{tt} r^3 S - 2a^2 g^{t\phi} r^3 S + 2g^{t\phi} r^6 S + a^2 g^{tt} S^2 - 2a^3 g^{t\phi} S^2 + a^4 g^{\phi\phi} S^2 - 2r^3 S^2 + 2a g^{t\phi} r^3 S^2 \\
&\quad - 2a^2 g^{\phi\phi} r^3 S^2 + g^{\phi\phi} r^6 S^2 + S^4 - 2F r^6 \beta + 4F r^3 S^2 \beta - 2F S^4 \beta + F^2 r^6 \beta^2 - 2F^2 r^3 S^2 \beta^2 + F^2 S^4 \beta^2).
\end{aligned}$$

Particles with angular momentum greater than the critical value experience a strong enough centrifugal force to prevent them from crossing into the BH's gravitational domain. Conversely, particles with angular momentum equal to or less than the critical value can overcome this barrier and spiral toward the event horizon, potentially leading to high-energy collisions or accretion [92].

This concept is fundamental in BH astrophysics for several reasons. For example, critical angular momentum determines which particles contribute to the accretion disk and which remain in distant orbits.

Particles with angular momentum near the critical value are most likely to collide near the event horizon, where the center-of-mass energy can be extremely high.

The dynamics governed by critical angular momentum influence observable phenomena, such as jet formation and radiation from accretion disks.

Figure 8 illustrates the dependence of the critical angular momentum of a rotating magnetized particle on the spin of the particle (s), the magnetic interaction parameter (β), and the spin of the Kerr BH (a). The figure consists of three panels, each showing how different physical parameters influence the motion of spinning magnetized particles near a Kerr BH immersed in an external magnetic field.

In the left panel, the variation with magnetic interaction parameter (β) is shown, displaying how the critical angular momentum of the test particle varies with the magnetic interaction parameter (β) for different values of the

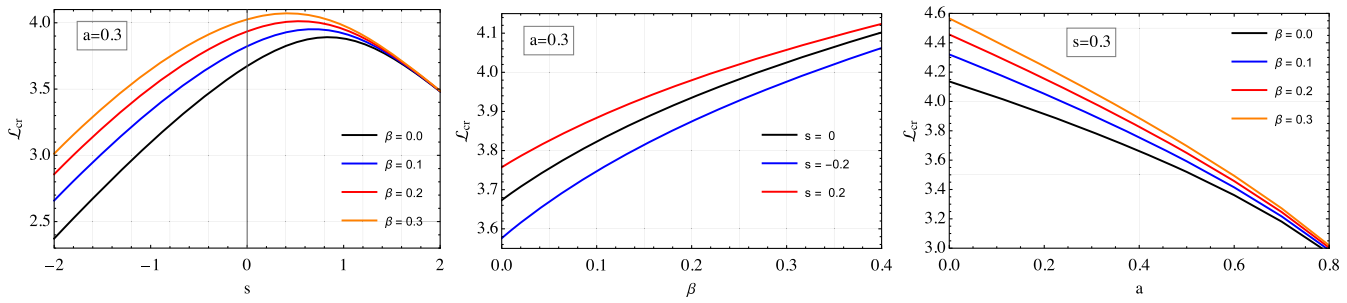

FIG. 8. Dependence of the critical angular momentum of a rotating magnetized particle on its spin (s), the magnetic interaction parameter (β), the BH spin (a), and $M = 1$. Higher BH rotation lowers the angular momentum barrier for infalling particles, facilitating collisions and energy release in magnetized Kerr systems.

particle's spin (s), keeping the BH spin fixed at a moderate value ($a = 0.3$). An increase in β leads to an increase in the critical angular momentum. Stronger magnetic interactions require a higher angular momentum for the particle to remain in orbit. Additionally, the effect is more pronounced for particles with larger spin values. In the middle panel, we illustrate the relationship between the critical angular momentum and the particle's spin (s) for different values of β while keeping the BH spin constant at $a = 0.3$. It is observed that, for small spin values ($s \approx 0$), the effect of the magnetic interaction is minimal. The interplay between spin-curvature coupling and magnetic interactions significantly modifies the required angular momentum for larger spin values. Retrograde spinning particles (negative s) tend to have lower critical angular momentum values compared to prograde spinning particles (positive s). In the right panel, we show the variation of critical angular momentum as a function of the BH spin (a) for different values of β, with the particle's spin fixed at $s = 0.3$. It is also observed that increasing the spin of a BH significantly reduces the required angular momentum for a given particle to maintain stable motion. This effect is particularly noticeable for high values of the magnetic interaction parameter (β). For rapidly rotating BHs ($a \approx 0.9$), the critical angular momentum decreases sharply due to the dominant frame-dragging effects. One may conclude from the findings in the figure that both spin and magnetic interactions play crucial roles in determining the stability of particles. Also, an increase of β may enhance the coupling between the particle's dipole moment and the external magnetic field, shifting the stability regions of circular motion. The BH spin acts as a stabilizing force for prograde orbits, lowering the required angular momentum for stable circular motion. The combined effects of spin-orbit coupling, magnetic dipole interactions, and frame-dragging must be considered in modeling particle motion around magnetized Kerr BHs.

B. Collisions of spinning magnetized particles

Assuming that two spinning magnetized particles approach the BH from infinity with identical energy-to-mass ratios ($\mathcal{E}_1/\mathcal{E}_2 = 1$), the center-of-mass energy ($\mathcal{E}_{\rm cm}$) of their collision can be derived. This energy depends on the particles' spins, magnetic interactions, and the BH's gravitational field.

In Schwarzschild spacetime (nonrotating BH), the calculation simplifies, but spin and magnetic interactions still significantly affect the result [93].

The center-of-mass energy is given by

$$E_{cm}^2 = -g^{\mu\nu}(p_\mu^{(1)} + p_\mu^{(2)})(p_\nu^{(1)} + p_\nu^{(2)}) = m_1^2 + m_2^2 - 2g^{\mu\nu}p_\mu^{(1)}p_\nu^{(2)}. \tag{58}$$

Here, $p_\mu^{(1)}$ and $p_\mu^{(2)}$ are the momentum of the first and second particle, respectively, given in Eqs. (28) and (29).

$$\mathcal{E}_{cm} = \frac{E_{cm}}{2m^2} = 1 - g^{tt}p_t^{(1)}p_t^{(2)} - g^{rr}p_r^{(1)}p_r^{(2)} - g^{\varphi\varphi}p_\varphi^{(1)}p_\varphi^{(2)} - g^{t\varphi}(p_t^{(1)}p_\varphi^{(2)} + p_\varphi^{(1)}p_t^{(2)}). \tag{59}$$

Here, $p_\mu^{(1)}$ and $p_\mu^{(2)}$ are the momentum of the first and second particle, respectively, given in Eqs. (28) and (29).

Spin and magnetic field effects modify these velocities, potentially leading to extremely high collision energies. The study of collisions between spinning magnetized particles near BHs has profound astrophysical significance. For example, the acceleration of particles to energies as high as 10^{22} eV near magnetized supermassive BHs could explain the most energetic cosmic rays detected on Earth [94].

High-energy collisions and interactions near BHs contribute to forming relativistic jets observed in active galactic nuclei (AGN) and quasars. Collisions of compact objects and extreme particle dynamics near BHs are potential sources of gravitational waves, detectable by observatories like LIGO and Virgo.

The collision of spinning magnetized particles near BHs presents a powerful mechanism for studying high-energy astrophysical processes and energy extraction. The BSW process, Penrose process, and magnetic Penrose process [93] provide theoretical frameworks to explore how BHs

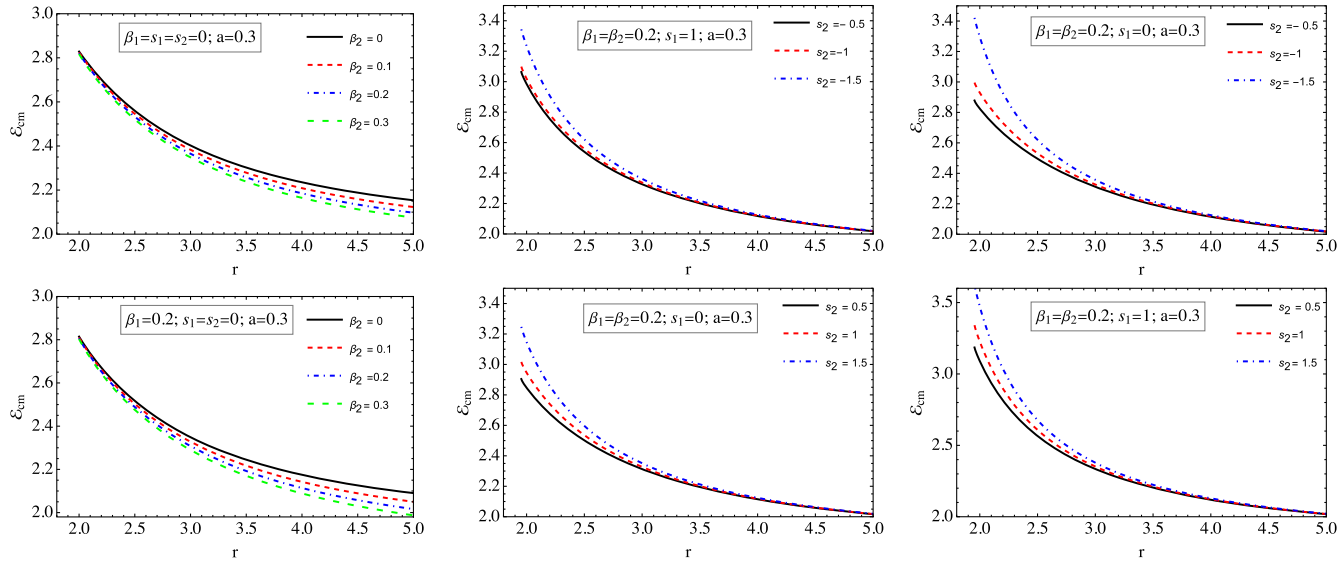

FIG. 9. Radial dependence of the center-of-mass energy of collisions of magnetized spinning particles motion with different s and β parameters. We take $M = 1$. Collisions yield ultrahigh energies close to the BH, supporting models of cosmic ray acceleration and gamma-ray bursts in spinning, magnetized environments.

can accelerate particles to extreme energies. Understanding the role of spin, magnetic fields, and critical angular momentum is essential for predicting and interpreting observable phenomena such as ultrahigh-energy cosmic rays, jet formation, and gravitational wave signals.

Figure 9 illustrates the center-of-mass energy (E_{cm}) for collisions of spinning magnetized particles in the vicinity of a Kerr BH. The analysis is conducted for different values of the particle's spin (s) and the magnetic interaction parameter (β), emphasizing how these factors influence high-energy collisions. The left panel presents the radial dependence of the center-of-mass energy for two colliding particles with different spin values. It is observed that as the particles approach the BH, the center-of-mass energy increases significantly. Higher spin values amplify the energy of the collisions, particularly in the near-horizon region. An external magnetic field enhances the center-of-mass energy, suggesting that strong magnetic interactions can contribute to the production of ultrahigh-energy cosmic rays.

This panel highlights the dependence of the center-of-mass energy on the magnetic interaction parameter (β) (see middle panel). Increasing β significantly enhances the energy of the collisions. Magnetic interactions enable greater energy amplification in the ergoregion, rendering this mechanism particularly relevant for astrophysical energy extraction processes. Finally, in the right panel, we explore how the Kerr BH's spin affects the energy of particle collisions. We have shown faster spinning BHs, which result in higher center-of-mass energy values. The combination of high spin and strong magnetic interactions

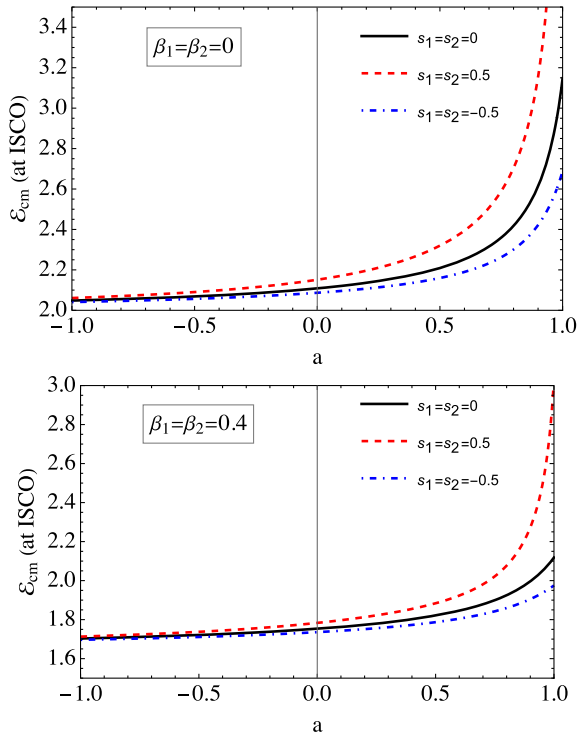

FIG. 10. The dependence of the center-of-mass energy of collisions of magnetized spinning particles at the ISCO on the BH spin parameter a for different s and β parameters. We take $M = 1$, and observe that energy maximizes at ISCO for aligned spins and moderate β. ISCO collisions in magnetized particles provide peak energy outputs, linking to efficient particle acceleration and radiation in active galactic nuclei.

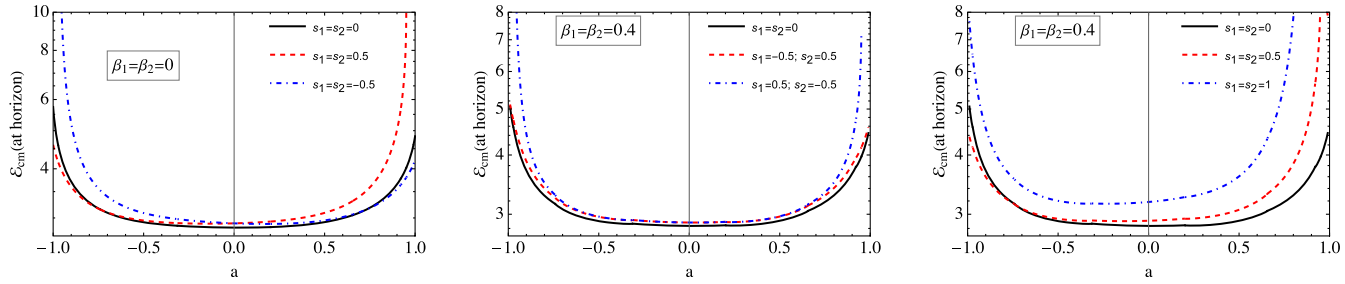

FIG. 11. The dependence of the center-of-mass energy of collisions of magnetized spinning particles at the event horizon on the BH spin parameter a for different s and β parameters. We take $M = 1$. Here, we consider all kinds of collisions: particles with the same spin orientation around corotating and counterrotating BHs. Energy increases with BH spin but decreases for opposite particle spins and magnetic interaction β.

yields extreme energy outputs, supporting scenarios in which BH magnetospheres accelerate particles to ultrarelativistic speeds.

In Fig. 10, we present the center-of-mass energy of colliding spinning-magnetized particles at ISCO with the angular momentum $\mathcal{L}_1 = -\mathcal{L}_2 = 2M$. It is observed that $\mathcal{E}_{cm}$ increases with the increase of the BH spin due to a decrease in the ISCO radius, while when the spin is negative, the energy decreases as the ISCO goes far from the central BH. The collisions of particles with the same spin direction are more energetic than those of particles with zero spin and opposite spin. Additionally, the presence of magnetic interaction causes a decrease in the center-of-mass energy. As the particles approach each other, their magnetic interaction energy increases, resulting in a loss of center-of-mass energy.

Now we analyse the center-of-mass energy at the horizon in Fig. 11. One can see from the dependence of the energy on the BH spin that it has a symmetry in cases of $a < 0$, positive spinning particle collisions ($s_i > 0$), and the case of $a > 0$, negative spinning particle ($s_i < 0$) collisions. Also, as large as the BH spin is, the particle's spin effects on the energy are significant. That means the BH and particle spin effects on the center-of-mass energy at the horizon support each other, enhancing the energy.

V. CONCLUSION

This study investigated the motion and collisions of spinning magnetized particles near a magnetized Kerr BH. Based on the MPD equations, our analysis offers new insights into the interplay between spin-orbit coupling, magnetic dipole interactions, and frame-dragging effects in strong gravitational fields. The key results of our study provide a new theoretical framework for understanding the behavior of magnetized test particles in astrophysical environments with strong magnetic fields.

One of the most significant findings is the modification of the ISCO and critical angular momentum due to the combined effects of spin and magnetic interactions. We found that the ISCO shifts outward with increasing magnetic interaction parameters, which suggests that strong magnetic interactions can stabilize orbits at larger radii. In contrast, the frame-dragging effect of the Kerr BH reduces the ISCO radius for prograde orbits, which means that spinning particles in strong magnetic fields can maintain stable circular motion much closer to the event horizon than previously thought. The critical angular momentum of a spinning magnetized particle increases with β, meaning that a higher angular momentum is required to counterbalance the effects of both the external magnetic field and the particle's intrinsic spin. Furthermore, we have discovered a new physical mechanism that can lead to an ultraefficient energy extraction process from Kerr BHs. Specifically, our results demonstrate that collisions of spinning magnetized particles can produce energy significantly exceeding the Bañados-Silk-West (BSW) limit. This enhancement occurs because the resonant interaction between spin-curvature coupling and the external magnetic field modifies the particle trajectories, thereby boosting the center-of-mass energy. The alignment or antialignment of the particle's spin with the BH's spin significantly affects the energy of the collision. In particular, particles with opposite spin orientations experience an amplified acceleration effect due to differential frame-dragging, leading to highly energetic collisions. This occurs when a spinning magnetized particle can effectively "extract" rotational energy from the BH and transfer it to the collision products by interacting with the external field. We have identified this as a novel energy extraction mechanism. One may explain that the interaction between the particle's spin and the Kerr BH's frame-dragging enhances energy transfer. Additionally, the external magnetic field alters the stability of orbits, enabling enhanced acceleration in specific resonance regions. The combination of spin-magnetic effects leads to highly energetic collisions, potentially generating particles with energy orders of magnitude higher than expected. This new process has direct astrophysical implications, particularly for ultrahigh-energy cosmic rays. The new mechanism could offer a natural explanation for the acceleration of cosmic rays to extreme energies that surpass the limits imposed by standard astrophysical accelerators.

Our findings may open new avenues for studying the interaction of magnetized plasmas and relativistic particles in the strong gravity regime of Kerr BHs. This study represents a significant step in understanding how spin and magnetism shape astrophysical processes near BHs. The new mechanism provides a fundamental mechanism for energy extraction, which may play a crucial role in the high-energy astrophysics of BHs, neutron stars, and magnetized compact objects. In contrast to our previous work on spinning magnetized particles around Schwarzschild BHs [56], this study extends the analysis to rotating Kerr BHs, revealing new effects due to BH spin and its interaction with particle spin and magnetic dipole moment. Our results show that the BH spin itself significantly alters the ISCO structure, shifting it inward for corotating orbits ($a > 0$) and outward for counterrotating orbits ($a < 0$), unlike the Schwarzschild case, where ISCO locations depend solely on spin and magnetic parameters. Furthermore, the combined effects of BH and particle spin (a, s) lead to highly asymmetric modifications in orbital dynamics, where positive spin particles ($s > 0$) experience a more substantial frame-dragging effect, resulting in a reduced ISCO radius. In contrast, negative spin particles ($s < 0$) counteract frame-dragging and shift ISCO outward. Additionally, the magnetic dipole moment and BH spin interaction (μ, a) introduce new features in the stability conditions of orbits—higher a values enhance the effect of magnetic repulsion, leading to a greater ISCO deviation compared to the Schwarzschild case. Notably, in the strong-field regime, the interplay of spin and magnetic interactions enables more efficient energy extraction via particle collisions, exceeding the energy amplification limits found in the Schwarzschild spacetime. These findings underscore the importance of considering BH spin when modeling astrophysical scenarios involving highly magnetized, spinning particles, such as pulsars and neutron stars orbiting supermassive BHs.

ACKNOWLEDGMENTS

Support for this research is given by Grant No. F-FA-2021-510 of the Uzbekistan Agency for Innovative Development. J. R. acknowledges the ERASMUS + ICM project for supporting their stay at the Silesian University in Opava.

DATA AVAILABILITY

The data are not publicly available. The data are available from the authors upon reasonable request.

[1] R. M. Wald, Phys. Rev. D **10**, 1680 (1974).
[2] G. Preti, Phys. Rev. D **70**, 024012 (2004).
[3] O. Kopáček, V. Karas, J. Kovář, and Z. Stuchlík, Astrophys. J. **722**, 1240 (2010).
[4] A. M. Al Zahrani, V. P. Frolov, and A. A. Shoom, Phys. Rev. D **87**, 084043 (2013).
[5] R. Shiose, M. Kimura, and T. Chiba, Phys. Rev. D **90**, 124016 (2014).
[6] R. Pánis, M. Kološ, and Z. Stuchlík, Eur. Phys. J. C **79**, 479 (2019).
[7] M. Akramov, C. Trunk, J. Yusupov, and D. Matrasulov, Europhys. Lett. **147**, 62001 (2024).
[8] Z. Stuchlík, M. Kološ, J. Kovář, P. Slaný, and A. Tursunov, Universe **6**, 26 (2020).
[9] K. Haydarov, J. Rayimbaev, A. Abdujabbarov, S. Palvanov, and D. Begmatova, Eur. Phys. J. C **80**, 399 (2020).
[10] S. U. Khan and Z.-M. Chen, Eur. Phys. J. C **83**, 760 (2023).
[11] S. Jumaniyozov, S. U. Khan, J. Rayimbaev, A. Abdujabbarov, and B. Ahmedov, Eur. Phys. J. C **84**, 291 (2024).
[12] J. Rayimbaev, A. Abdujabbarov, D. Bardiev, B. Ahmedov, and M. Abdullaev, Eur. Phys. J. Plus **138**, 358 (2023).
[13] F. C. Michel and H. Li, Phys. Rep. **318**, 227 (1999).
[14] J. Rayimbaev, S. Jumaniyozov, M. Umaraliyev, and A. Abdujabbarov, Universe **8**, 496 (2022).
[15] Z. Stuchlík, M. Kološ, and A. Tursunov, Universe **7**, 416 (2021).
[16] S. U. Khan, O. Abdurkhmonov, J. Rayimbaev, S. Ahmedov, Y. Turaev, and S. Muminov, Eur. Phys. J. C **84**, 650 (2024).
[17] F. de Felice and F. Sorge, Classical Quantum Gravity **20**, 469 (2003).
[18] F. de Felice, F. Sorge, and S. Zilio, Classical Quantum Gravity **21**, 961 (2004).
[19] D. Pugliese, H. Quevedo, and R. Ruffini, Phys. Rev. D **83**, 104052 (2011).
[20] D. Pugliese, H. Quevedo, and R. Ruffini, Phys. Rev. D **88**, 024042 (2013).
[21] S. U. Khan and J. Ren, in *American Institute of Physics Conference Series* (AIP Publishing, Melville, New York, 2021), Vol. 2319, p. 040005.
[22] S. U. Khan and J. Ren, Chin. J. Phys. **78**, 141 (2022).
[23] S. Jumaniyozov, M. Zahid, M. Alloqulov, I. Ibragimov, J. Rayimbaev, and S. Murodov, Eur. Phys. J. C **85**, 126 (2025).
[24] V. P. Frolov and A. A. Shoom, Phys. Rev. D **82**, 084034 (2010).
[25] I. Kaygorodov, A. Khudoyberdiyev, and Z. Shermatova, J. Geom. Phys. **207**, 105356 (2025).
[26] J. Rayimbaev, A. Abdujabbarov, B. Turimov, and F. Atamurotov, arXiv:2004.10031.

[27] A. N. Aliev and N. Özdemir, Mon. Not. R. Astron. Soc. **336**, 241 (2002).
[28] S. U. Khan and Z.-M. Chen, Chin. J. Phys. **92**, 1659 (2024).
[29] S. U. Khan, J. Rayimbaev, F. Sarikulov, and O. Abdurakhmonov, Chin. J. Phys. **90**, 690 (2024).
[30] S. U. Khan, U. Uktamov, J. Rayimbaev, A. Abdujabbarov, I. Ibragimov, and Z.-M. Chen, Eur. Phys. J. C **84**, 203 (2024).
[31] B. Toshmatov, O. Rahimov, B. Ahmedov, and A. Ahmedov, Galaxies **9**, 65 (2021).
[32] B. Ahmedov, O. Rahimov, and B. Toshmatov, Universe **7**, 307 (2021).
[33] O. Rahimov, B. Toshmatov, Y. Vyblyi, A. Akhmedov, and B. Abdulazizov, Phys. Dark Universe **44**, 101483 (2024).
[34] B. Turimov and O. Rahimov, Universe **8**, 507 (2022).
[35] B. Turimov, O. Rahimov, B. Ahmedov, Z. Stuchlík, and K. Boymurodova, Int. J. Mod. Phys. D **30**, 2150037 (2021).
[36] B. Turimov, A. Mamadjanov, and O. Rahimov, Galaxies **11**, 70 (2023).
[37] S. Suzuki and K.-I. Maeda, Phys. Rev. D **58**, 023005 (1998).
[38] N. I. Shakura and R. A. Sunyaev, Astron. Astrophys. **24**, 337 (1973).
[39] M. A. Abramowicz and P. C. Fragile, Living Rev. Relativity **16**, 1 (2013).
[40] M. Abramowicz, M. Jaroszynski, and M. Sikora, Astron. Astrophys. **63**, 221 (1978).
[41] Event Horizon Telescope Collaboration, Astron. Astrophys. Lett. **875**, L1 (2019).
[42] R. Penrose, Nuovo Cimento Riv. Ser. **1**, 252 (1969).
[43] R. Penrose and R. M. Floyd, Nat. Phys. Sci. **229**, 177 (1971).
[44] R. D. Blandford and R. L. Znajek, Mon. Not. R. Astron. Soc. **179**, 433 (1977).
[45] N. Dadhich, A. Tursunov, B. Ahmedov, and Z. Stuchlík, Mon. Not. R. Astron. Soc. **478**, L89 (2018).
[46] S. Wagh, S. Dhurandhar, and N. Dadhich, Astrophys. J. **290**, 12 (1985).
[47] Y. Du, Y. Liu, and X. Zhang, Eur. Phys. J. C **82**, 871 (2022).
[48] M. Akramov, B. Eshchanov, S. Usanov, S. Norbekov, and D. Matrasulov, Phys. Lett. A **524**, 129827 (2024).
[49] S. Mukherjee, Phys. Lett. B **778**, 54 (2018).
[50] S. U. Khan and J. Ren, Chin. J. Phys. **70**, 55 (2021).
[51] A. Tursunov, B. Juraev, Z. Stuchlík, and M. Kološ, Phys. Rev. D **104**, 084099 (2021).
[52] Z. Stuchlík, M. Kološ, and A. Tursunov, Universe **7**, 416 (2021).
[53] M. Bañados, J. Silk, and S. M. West, Phys. Rev. Lett. **103**, 111102 (2009).
[54] M. Zahid, S. U. Khan, J. Ren, and J. Rayimbaev, Int. J. Mod. Phys. D **31**, 2250058 (2022).
[55] M. Zahid, J. Rayimbaev, S. U. Khan, J. Ren, S. Ahmedov, and I. Ibragimov, Eur. Phys. J. C **82**, 494 (2022).
[56] F. Abdulxamidov, J. Rayimbaev, A. Abdujabbarov, and Z. Stuchlík, Phys. Rev. D **108**, 044030 (2023).
[57] A. A. Deriglazov and W. Guzmán Ramírez, Adv. Theor. Math. Phys. **2017**, 7397159 (2017).
[58] A. A. Deriglazov and W. Guzmán Ramírez, Phys. Lett. B **779**, 210 (2018).
[59] L. Costa, J. Natario, and M. Zilhão, Phys. Rev. D **93**, 104006 (2012).
[60] A. H. Bokhari, J. Rayimbaev, and B. Ahmedov, Phys. Rev. D **102**, 124078 (2020).
[61] M. Mathisson, Acta Phys. Pol. **6**, 163 (1937).
[62] A. Papapetrou, Proc. R. Soc. A **209**, 248 (1951).
[63] E. Corinaldesi and A. Papapetrou, Proc. R. Soc. A **209**, 259 (1951).
[64] W. G. Dixon, Commun. Math. Phys. **1**, 1 (1964).
[65] M. Mathisson, Z. Phys. **108**, 29 (1937).
[66] F. A. E. Pirani, Acta Phys. Pol. **15**, 389 (1956).
[67] E. Corinaldesi and A. Papapetrou, Proc. R. Soc. A **251**, 529 (1959).
[68] A. Papapetrou, Proc. R. Soc. A **209**, 248 (1961).
[69] J. Poitou, C. R. Acad. Sci. Paris **272**, 703 (1971).
[70] B. Tulzcyjew, Acta Phys. Pol. **18**, 393 (1959).
[71] B. Tulzcyjew and W. Tulzcyjew, Zeitschrift Angewandte Mathematik und Mechanik **43**, 247 (1962).
[72] W. G. Dixon, Nuovo Cimento (1955–1965) **34**, 317 (1964).
[73] W. G. Dixon, Proc. R. Soc. A **314**, 499 (1970).
[74] W. G. Dixon, Proc. R. Soc. A **319**, 509 (1970).
[75] J. Ehlers and E. Rudolph, Gen. Relativ. Gravit. **8**, 197 (1977).
[76] V. P. Frolov and A. A. Shoom, Phys. Rev. D **82**, 084034 (2010).
[77] A. Tursunov, Z. Stuchlík, and M. Kološ, Phys. Rev. D **93**, 084012 (2016).
[78] B. Toshmatov, O. Rahimov, B. Ahmedov, and D. Malafarina, Eur. Phys. J. C **80**, 675 (2020).
[79] C. A. Benavides-Gallego, A. Abdujabbarov, D. Malafarina, B. Ahmedov, and C. Bambi, Phys. Rev. D **99**, 044012 (2019).
[80] F. Abdulxamidov, C. A. Benavides-Gallego, W.-B. Han, J. Rayimbaev, and A. Abdujabbarov, Phys. Rev. D **106**, 024012 (2022).
[81] J. M. Ladino and E. Larrañaga, Int. J. Mod. Phys. D **31**, 2250091 (2022).
[82] S. A. Hojman and F. A. Asenjo, Classical Quantum Gravity **30**, 025008 (2013).
[83] J. M. Bardeen, W. H. Press, and S. A. Teukolsky, Astrophys. J. **178**, 347 (1972).
[84] C. W. Misner, K. S. Thorne, and J. A. Wheeler, *Gravitation* (W. H. Freeman and Company, San Francisco, 1973), a comprehensive resource for the theoretical foundations of general relativity.
[85] S. Jumaniyozov, S. Khan, J. Rayimbaev *et al.*, Eur. Phys. J. C **84**, 964 (2024).
[86] S. L. Shapiro and S. A. Teukolsky, *Essential Textbook for Understanding Compact Objects in Relativistic Astrophysics* (John Wiley & Sons, New York, 1983).
[87] I. D. Novikov and K. S. Thorne, *Black Holes (Les Astres Occlus)* (Gordon and Breach, NY, 1973), provides in-depth exploration of Kerr black hole properties.
[88] V. P. Frolov and I. Novikov, *Black Hole Physics* (Springer, Dordrecht, 1998).
[89] D. C. Wilkins, Phys. Rev. D **5**, 814 (1972).
[90] M. Bañados, J. Silk, and S. M. West, Phys. Rev. Lett. **103**, 111102 (2009).
[91] V. Cardoso, A. S. Miranda, E. Berti, H. Witek, and V. T. Zanchin, Phys. Rev. D **79**, 064016 (2009).
[92] S. Chandrasekhar, *The Mathematical Theory of Black Holes* (Oxford University Press, New York, 1983).
[93] R. M. Wald, Astrophys. J. **191**, 231 (1974).
[94] K. S. Thorne, Astrophys. J. **191**, 507 (1974).